Wind and Structures, Vol. 7, No. 6 (2004) 421-447
DOI: http://dx.doi.org/10.12989/was.2004.7.6.421

Time domain buffeting analysis of long suspension bridges under skew winds

G. Liu† and Y. L. Xu‡

Department of Civil and Structural Engineering, The Hong Kong Polytechnic University, Hung Hom, Kowloon, Hong Kong, China

L. D. Zhu‡

State Key Laboratory for Disaster Reduction in Civil Engineering and Department of Bridge Engineering, Tongji University, Shanghai 200092, China

(Received July 30, 2003, Accepted September 23, 2004)

Abstract. This paper presents a time domain approach for predicting buffeting response of long suspension bridges under skew winds. The buffeting forces on an oblique strip of the bridge deck in the mean wind direction are derived in terms of aerodynamic coefficients measured under skew winds and equivalent fluctuating wind velocities with aerodynamic impulse functions included. The time histories of equivalent fluctuating wind velocities and then buffeting forces along the bridge deck are simulated using the spectral representation method based on the Gaussian distribution assumption. The self-excited forces on an oblique strip of the bridge deck are represented by the convolution integrals involving aerodynamic impulse functions and structural motions. The aerodynamic impulse functions of self-excited forces are derived from experimentally measured flutter derivatives under skew winds using rational function approximations. The governing equation of motion of a long suspension bridge under skew winds is established using the finite element method and solved using the Newmark numerical method. The proposed time domain approach is finally applied to the Tsing Ma suspension bridge in Hong Kong. The computed buffeting responses of the bridge under skew winds during Typhoon Sam are compared with those obtained from the frequency domain approach and the field measurement. The comparisons are found satisfactory for the bridge response in the main span.

Keywords: long suspension bridge; skew winds; buffeting response; time domain; equivalent turbulent wind velocity; field measurement; Typhoon Sam; comparison.

1. Introduction

The prediction of wind-induced buffeting response is practically important for design, construction, and structural health monitoring of long suspension bridges. The field measurements of long suspension bridges during strong winds manifest that mean wind direction relative to a bridge deck often deviates from the normal of a bridge deck (Xu, *et al*. 2000). However, the traditional buffeting

† Research Associate
‡ Professor

analysis often assumes that mean wind is coming at a right angle to the longitudinal axis of the bridge deck. This leads to some technical difficulties in performing a satisfactory comparison of buffeting response between field measurements and analyses. Furthermore, if a little more realistic prediction of buffeting response is to be made in relation to local wind climate, the directionality of wind needs to be taken into account and the buffeting analysis of the bridge under skew winds becomes necessary (Kimura and Tanaka 1992). Thus, for a better prediction of buffeting response of a long suspension bridge and a reasonable comparison with field measurement results, it is worthwhile to seek proper analytical approaches for buffeting response prediction of long suspension bridges under skew winds.

Analytical approach for buffeting response prediction of long suspension bridges has predominantly been conducted in the frequency domain (Davenport 1962, Scanlan 1978). The frequency domain approach was developed based on the quasi-steady assumption. It has evolved in the past two decades to include self-excited forces in the lateral direction, aerodynamic admittance functions, multi-mode effects, and inter-mode coupling effects (Scanlan and Jones 1990, Jain, *et al*. 1996, Xu, *et al*. 1998, Chen, *et al*. 2000a). Furthermore, the frequency domain approach for buffeting response prediction of long span bridges under skew winds has also been fulfilled (Zhu 2002a, Xu, *et al*. 2003). The frequency domain approach has fast computational efficiency and can conveniently handle the aerodynamic admittances functions and flutter derivatives that are functions of frequency. However, the frequency domain approach is limited to linear structural systems excited by stationary wind forces without aerodynamic nonlinearities.

With the rapid development of computer technology and computational method, analytical approach in the time domain for buffeting response prediction of long suspension bridges has been developed rapidly. The self-excited forces were introduced in the time domain approach through aerodynamic impulse functions associated with flutter derivatives (Bucher and Lin 1988, Xiang, *et al*. 1995). Chen, *et al*. (2000b) further incorporated aerodynamic admittance functions in the time domain approach through their counterparts-aerodynamic impulse functions. However, the aforementioned time domain approaches assume that mean wind is coming at a right angle to the longitudinal axis of the bridge deck.

In this study, a time domain approach for predicting the buffeting response of long suspension bridges under skew winds is presented. The buffeting forces on an oblique strip of the bridge deck in the mean wind direction are derived in terms of aerodynamic coefficients measured under skew winds and equivalent fluctuating wind velocities with aerodynamic impulse functions included. The time histories of equivalent fluctuating wind velocities and then buffeting forces along the bridge deck are simulated using the spectral representation method based on the Gaussian distribution assumption. The self-excited forces on an oblique strip of the bridge deck are represented by the convolution integrals involving aerodynamic impulse functions and structural motions. The aerodynamic impulse functions of self-excited forces are derived from experimentally measured flutter derivatives under skew winds using rational function approximations. The governing equation of motion of a long suspension bridge under skew winds is established using the finite element method and solved using the Newmark numerical method. The proposed time domain approach is finally applied to the Tsing Ma suspension bridge in Hong Kong. The computed buffeting responses of the bridge under skew winds during Typhoon Sam are compared with those obtained from the frequency domain approach and the field measurement.

2. Formulation

2.1. Governing equation of motion for bridge buffeting due to skew winds

In the proposed time domain buffeting analysis of long suspension bridges under skew winds, the three-dimensional finite element approach is employed to establish the governing equation of motion of the bridge under skew winds. The governing equation of motion of a suspension bridge under skew winds can be expressed as

$$\boldsymbol{M}^s \ddot{\boldsymbol{\Delta}}(t) + \boldsymbol{C}^s \dot{\boldsymbol{\Delta}}(t) + \boldsymbol{K}^s \boldsymbol{\Delta}(t) = \boldsymbol{F}^{bu}(t) + \boldsymbol{F}^{se}(t) \tag{1}$$

where $\boldsymbol{M}^s$, $\boldsymbol{C}^s$ and $\boldsymbol{K}^s$ are, respectively, the $N \times N$ mass, damping, and stiffness matrices of the entire bridge; $\boldsymbol{F}^{bu}(t)$ and $\boldsymbol{F}^{se}(t)$ are, respectively, the buffeting and self-excited force vectors of N dimensions due to skew winds, $\boldsymbol{\Delta}(t)$ is the global nodal displacement vector of N-dimensions; and N is the number of the total degrees of freedom of the entire bridge.

2.2. Buffeting forces due to skew winds

When employing the finite element method to describe the vibration problem of a long suspension bridge excited by buffeting forces due to skew winds, a set of coordinate systems should be properly established. A global structural coordinate system XYZ should be set up to consider the overall dynamic equilibrium conditions of the bridge. A global wind coordinate system $X_u Y_v Z_w$ is required to define the mean wind velocity and turbulent wind. The two global coordinate systems are then correlated through the global wind yaw angle and inclination. In Fig. 1(a), the axis X_u is set along the direction of the mean wind $\overline{U}$. The axis Y_v is parallel to the X-Y plane. The axis Z_w is upward and perpendicular to the axes X_u and Y_v following a right-hand rule. The positive directions of the three axes X_u, Y_v and Z_w represent the positive directions of velocity fluctuations $u(t)$, $v(t)$ and $w(t)$, respectively. The angles β_0 and θ_0 are used to define the global yaw angle and inclination of the mean wind $\overline{U}$ with respect to the XYZ-system.

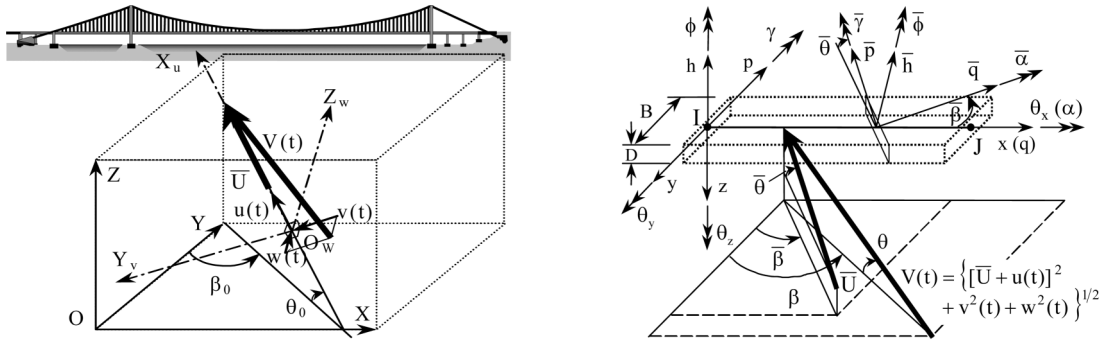

Fig. 1 Global and local coordinate systems

With the use of the finite element method, a local structural coordinate system *xyz*, referring to the static equilibrium position of the bridge, is required for each element to define the matrices of elemental mass, stiffness, damping, and loading. Furthermore, the aerodynamic coefficients and flutter derivatives of the bridge deck under skew winds are measured through wind tunnel tests, in which wind yaw angle and inclination are often defined with respect to local wind and reference coordinate systems. The measured coefficients are then expressed as the function of local mean wind yaw angle and inclination. Thus, it is necessary to introduce a local reference coordinate *qph*-system and a local wind coordinate $\overline{qph}$-system. Fig. 1(b) shows the three local coordinate systems. The angles $\overline{\beta}$ and $\overline{\theta}$ are used to define the local yaw angle and inclination of the mean wind $\overline{U}$ in the *qph*-system. The angles $\beta(t)$ and $\theta(t)$ are, respectively, the local yaw angle and inclination of the transient wind speed $V(t)$ in the *qph*-system.

It is not difficult to establish the 3×3 transformation matrix $\boldsymbol{T}_{LrGw}$ from the $X_uY_vZ_w$-system to the *qph*-system. Then, the local yaw angle and inclination $\overline{\beta}$ and $\overline{\theta}$ and their increments $\Delta\beta(t)$ and $\Delta\theta(t)$ in the *qph*-system can be derived and expressed as follows after a linearization.

$$\overline{\beta} = \tan^{-1}(-t_{11}/t_{21}); \quad \overline{\theta} = \tan^{-1}(t_{31}/\sqrt{t_{11}^2 + t_{21}^2}) \tag{2}$$

$$\Delta\beta = \beta(t) - \overline{\beta} \approx \frac{t_{11}t_{22} - t_{12}t_{21}}{t_{11}^2 + t_{21}^2}\frac{v(t)}{\overline{U}} + \frac{t_{11}t_{23} - t_{13}t_{21}}{t_{11}^2 + t_{21}^2}\frac{w(t)}{\overline{U}} \tag{3}$$

$$\Delta\theta = \theta(t) - \overline{\theta} \approx \frac{t_{32}}{\sqrt{t_{11}^2 + t_{21}^2}}\frac{v(t)}{\overline{U}} + \frac{t_{33}}{\sqrt{t_{11}^2 + t_{21}^2}}\frac{w(t)}{\overline{U}} \tag{4}$$

where $\Delta\beta(t)$ and $\Delta\theta(t)$ are the time-dependent increments of the local yaw angle and inclination due to the fluctuations of wind velocity; and t_{ij} is the element of the *i*th row and *j*th column of the matrix $\boldsymbol{T}_{LrGw}$. The aerodynamic forces acting on the structural element due to the transient wind speed $V(t)$ can then be expressed as the function of $\Delta\beta(t)$, $\Delta\theta(t)$, $u(t)$, $v(t)$, $w(t)$, $\overline{U}$, and the aerodynamic coefficients of the element with respect to $\overline{\beta}$ and $\overline{\theta}$. By assuming that the fluctuating wind components are much smaller than the mean wind speed, that is, low turbulence intensities, the non-linear terms of $u(t)$, $v(t)$ and $w(t)$ can be ignored (Holmes 2001). Finally, by performing a series of coordinate transformations, the buffeting forces due to skew winds in the global structural coordinate system can be found

$$\boldsymbol{F}^{bu}(t) = \sum_{i=1}^{n} \boldsymbol{T}_i^{bu}\overline{\boldsymbol{F}}_i^{bu}(t) \tag{5}$$

where $\overline{\boldsymbol{F}}_i^{bu}(t)$ is the 12×1 vector of buffeting forces at the nodes of the *i*th element with respect to the global structural coordinate *XYZ*-system; $\boldsymbol{T}_i^{bu}(i = 1, \ldots, n)$ is the N×12 matrix with its elements being either zero or unit to locate the vector $\overline{\boldsymbol{F}}_i^{bu}(t)$ at the proper position in the global vector $\boldsymbol{F}^{bu}(t)$; and n is the number of the total elements on which the buffeting forces need to be accounted. The expression of $\overline{\boldsymbol{F}}_i^{bu}(t)$ can be written as

$$\overline{\boldsymbol{F}}_i^{bu}(t) = \overline{\boldsymbol{T}}_{GsLs,i}\tilde{\boldsymbol{N}}_i^T\boldsymbol{T}_{LsL\overline{w},i}\overline{\boldsymbol{P}}_i^{bu}(t) \tag{6}$$

where $\overline{\boldsymbol{P}}_i^{bu}(t)$ is the 6×1 vector of buffeting forces per unit length of the *i*th oblique strip (element)

of the bridge deck with respect to the local mean wind coordinate $\overline{qph}$-system; $\boldsymbol{T}_{LsL\bar{w},i}$ is the 6×6 transformation matrix from the local wind coordinate system $\overline{qph}$ to the local structural coordinate system *xyz* for the *i*th element; $\tilde{\boldsymbol{N}}_i$ is the 6×12 matrix of the displacement interpolation functions of the *i*th element as used in the conventional finite element method; $\bar{\boldsymbol{T}}_{GsLs,i}$ is the 12×12 transformation matrix from the local *xyz*-system to the global *XYZ*-system for the *i*th element.

The vector $\bar{\boldsymbol{P}}_i^{bu}(t)$ is the function of the air density ρ, the element width B_i, the mean wind speed at the center of the element $\bar{U}_i$, the fluctuations of wind velocity at the center of the element $u_i(t)$, $v_i(t)$ and $w_i(t)$, the aerodynamic impulse functions of the element under skew winds, the aerodynamic coefficients and their derivatives of the element under skew winds, the coordinate transformation matrix $\boldsymbol{T}_{LrGw,i}$, and others. The resulting expression is as follows

$$\bar{\boldsymbol{P}}_i^{bu}(t) = \begin{bmatrix} C_{\bar{q},i}^{bu}(t) \\ D_{\bar{p},i}^{bu}(t) \\ L_{\bar{h},i}^{bu}(t) \\ M_{\bar{\alpha},i}^{bu}(t) \\ M_{\bar{\gamma},i}^{bu}(t) \\ M_{\bar{\phi},i}^{bu}(t) \end{bmatrix} = \frac{\rho \bar{U}_i B_i}{2} \begin{bmatrix} a_{11}u_{C_{\bar{q},i}^{bu},eq}(t) + a_{12}v_{C_{\bar{q},i}^{bu},eq}(t) + a_{13}w_{C_{\bar{q},i}^{bu},eq}(t) \\ a_{21}u_{D_{\bar{p},i}^{bu},eq}(t) + a_{22}v_{D_{\bar{p},i}^{bu},eq}(t) + a_{23}w_{D_{\bar{p},i}^{bu},eq}(t) \\ a_{31}u_{L_{\bar{h},i}^{bu},eq}(t) + a_{32}v_{L_{\bar{h},i}^{bu},eq}(t) + a_{33}w_{L_{\bar{h},i}^{bu},eq}(t) \\ a_{41}u_{M_{\bar{\alpha},i}^{bu},eq}(t) + a_{42}v_{M_{\bar{\alpha},i}^{bu},eq}(t) + a_{43}w_{M_{\bar{\alpha},i}^{bu},eq}(t) \\ a_{51}u_{M_{\bar{\gamma},i}^{bu},eq}(t) + a_{52}v_{M_{\bar{\gamma},i}^{bu},eq}(t) + a_{53}w_{M_{\bar{\gamma},i}^{bu},eq}(t) \\ a_{61}u_{M_{\bar{\phi},i}^{bu},eq}(t) + a_{62}v_{M_{\bar{\phi},i}^{bu},eq}(t) + a_{63}w_{M_{\bar{\phi},i}^{bu},eq}(t) \end{bmatrix} \tag{7}$$

where $C_{\bar{q},i}^{bu}(t)$, $D_{\bar{p},i}^{bu}(t)$, $L_{\bar{h},i}^{bu}(t)$, $M_{\bar{\alpha},i}^{bu}(t)$, $M_{\bar{\gamma},i}^{bu}(t)$ and $M_{\bar{\phi},i}^{bu}(t)$ are the buffeting crosswind force, drag, lift, pitching moment, rolling moment, and yawing moment on the *i*th oblique element of the bridge deck with respect to the local wind coordinate $\overline{qph}$ system, respectively; a_{jk} ($j = 1, 2, ..., 6$; $k = 1, 2, ..., 3$) are the coefficients, which are the function of aerodynamic coefficients and their derivatives of the element under skew winds and the coordinate transformation matrix $\boldsymbol{T}_{LrGw,i}$(see Appendix A); and $u_{\bar{P}_i^{bu},eq}(t)$, $v_{\bar{P}_i^{bu},eq}(t)$, $w_{\bar{P}_i^{bu},eq}(t)$ ($\bar{P}_i^{bu} = C_{\bar{q},i}^{bu}, D_{\bar{p},i}^{bu}, L_{\bar{h},i}^{bu}, M_{\bar{\alpha},i}^{bu}, M_{\bar{\gamma},i}^{bu}$ and $M_{\bar{\phi},i}^{bu}$) are six sets of equivalent fluctuating wind velocities defined as follows

$$\{u_{C_{\bar{q},i}^{bu},eq}(t)\ v_{C_{\bar{q},i}^{bu},eq}(t)\ w_{C_{\bar{q},i}^{bu},eq}(t)\}^T = \left\{\int_{-\infty}^{t} I_{C_{\bar{q},i}^{bu,u}}(t-\tau)u_i(\tau)d\tau \quad \int_{-\infty}^{t} I_{C_{\bar{q},i}^{bu,v}}(t-\tau)v_i(\tau)d\tau \quad \int_{-\infty}^{t} I_{C_{\bar{q},i}^{bu,w}}(t-\tau)w_i(\tau)d\tau\right\}^T \tag{8}$$

$$\{u_{D_{\bar{p},i}^{bu},eq}(t)\ v_{D_{\bar{p},i}^{bu},eq}(t)\ w_{D_{\bar{p},i}^{bu},eq}(t)\}^T = \left\{\int_{-\infty}^{t} I_{D_{\bar{p},i}^{bu,u}}(t-\tau)u_i(\tau)d\tau \quad \int_{-\infty}^{t} I_{D_{\bar{p},i}^{bu,v}}(t-\tau)v_i(\tau)d\tau \quad \int_{-\infty}^{t} I_{D_{\bar{p},i}^{bu,w}}(t-\tau)w_i(\tau)d\tau\right\}^T \tag{9}$$

$$\{u_{L_{\bar{h},i}^{bu},eq}(t)\ v_{L_{\bar{h},i}^{bu},eq}(t)\ w_{L_{\bar{h},i}^{bu},eq}(t)\}^T = \left\{\int_{-\infty}^{t} I_{L_{\bar{h},i}^{bu,u}}(t-\tau)u_i(\tau)d\tau \quad \int_{-\infty}^{t} I_{L_{\bar{h},i}^{bu,v}}(t-\tau)v_i(\tau)d\tau \quad \int_{-\infty}^{t} I_{L_{\bar{h},i}^{bu,w}}(t-\tau)w_i(\tau)d\tau\right\}^T \tag{10}$$

$$\{u_{M_{\bar{\alpha},i}^{bu},eq}(t)\ v_{M_{\bar{\alpha},i}^{bu},eq}(t)\ w_{M_{\bar{\alpha},i}^{bu},eq}(t)\}^T = \left\{\int_{-\infty}^{t} I_{M_{\bar{\alpha},i}^{bu,u}}(t-\tau)u_i(\tau)d\tau \quad \int_{-\infty}^{t} I_{M_{\bar{\alpha},i}^{bu,v}}(t-\tau)v_i(\tau)d\tau \quad \int_{-\infty}^{t} I_{M_{\bar{\alpha},i}^{bu,w}}(t-\tau)w_i(\tau)d\tau\right\}^T \tag{11}$$

$$\{u_{M_{\bar{\gamma},i}^{bu},eq}(t)\ v_{M_{\bar{\gamma},i}^{bu},eq}(t)\ w_{M_{\bar{\gamma},i}^{bu},eq}(t)\}^T = \left\{\int_{-\infty}^{t} I_{M_{\bar{\gamma},i}^{bu,u}}(t-\tau)u_i(\tau)d\tau \quad \int_{-\infty}^{t} I_{M_{\bar{\gamma},i}^{bu,v}}(t-\tau)v_i(\tau)d\tau \quad \int_{-\infty}^{t} I_{M_{\bar{\gamma},i}^{bu,w}}(t-\tau)w_i(\tau)d\tau\right\}^T \tag{12}$$

$$\{u_{M_{\bar{\phi},i}^{bu},eq}(t)\ v_{M_{\bar{\phi},i}^{bu},eq}(t)\ w_{M_{\bar{\phi},i}^{bu},eq}(t)\}^T = \left\{\int_{-\infty}^{t} I_{M_{\bar{\phi},i}^{bu,u}}(t-\tau)u_i(\tau)d\tau \quad \int_{-\infty}^{t} I_{M_{\bar{\phi},i}^{bu,v}}(t-\tau)v_i(\tau)d\tau \quad \int_{-\infty}^{t} I_{M_{\bar{\phi},i}^{bu,w}}(t-\tau)w_i(\tau)d\tau\right\}^T \tag{13}$$

where the superscript "T" represents the matrix operation of transpose; and $I_{\bar{P}_i^{bu,u}}(t-\tau)$, $I_{\bar{P}_i^{bu,v}}(t-\tau)$ and $I_{\bar{P}_i^{bu,w}}(t-\tau)$ ($\bar{P}_i^{bu} = C_{\bar{q},i}^{bu}, D_{\bar{p},i}^{bu}, L_{\bar{h},i}^{bu}, M_{\bar{\alpha},i}^{bu}, M_{\bar{\gamma},i}^{bu}$ and $M_{\bar{\phi},i}^{bu}$) are the aerodynamic impulse functions of the ith oblique element. Eqs. (8) to (13) indicate that six sets of equivalent turbulent wind velocities are needed to describe the corresponding six-component buffeting forces.

Clearly, the equivalent turbulent wind velocities are linear transformations of the turbulent wind velocities $u(t)$, $v(t)$ and $w(t)$. Therefore, the equivalent turbulent wind velocities also follow the Gaussian distribution if the turbulent wind velocities follow the Gaussian distribution. Non-Gaussian distribution of the turbulent wind velocities is not considered in this study because of the comparison with the results from the frequency domain approach which is based on the Gaussian distribution assumption. Each set of equivalent turbulent wind velocities along the bridge deck can be simulated using the spectral representation method (Shinozuka and Deodatis 1991, Deodatis 1996). Let us take the equivalent turbulent wind velocities associated with the drag force as an example. The equivalent turbulent wind velocities along the bridge deck in the lateral direction can be expressed as a three-dimensional multivariate stochastic process.

$$\boldsymbol{f}_{D_{\bar{p}}^{bu},eq}(t) = \{u_{D_{\bar{p},1}^{bu},eq}(t)\ \ v_{D_{\bar{p},1}^{bu},eq}(t)\ \ w_{D_{\bar{p},1}^{bu},eq}(t)\ \ \ldots\ldots\ u_{D_{\bar{p},n}^{bu},eq}(t)\ \ v_{D_{\bar{p},n}^{bu},eq}(t)\ \ w_{D_{\bar{p},n}^{bu},eq}(t)\}^T \tag{14}$$

The cross spectral density matrix of $\boldsymbol{f}_{D_{\bar{p}}^{bu},eq}(t)$ is a $3n \times 3n$ matrix $\boldsymbol{S}_{D_{\bar{p}}^{bu}}^0(\omega)$ given by

$$\boldsymbol{S}_{D_{\bar{p}}^{bu}}^0(\omega) = \begin{bmatrix} \boldsymbol{S}_{D_{\bar{p}}^{bu},11}(\omega) & \cdots & \boldsymbol{S}_{D_{\bar{p}}^{bu},1n}(\omega) \\ \cdots & \ddots & \cdots \\ \boldsymbol{S}_{D_{\bar{p}}^{bu},n1}(\omega) & \cdots & \boldsymbol{S}_{D_{\bar{p}}^{bu},nn}(\omega) \end{bmatrix} \tag{15}$$

$$\boldsymbol{S}_{D_{\bar{p}}^{bu},jk}(\omega) = \begin{bmatrix} S_{D_{\bar{p}}^{bu},eq,uu}(P_j, P_k, \omega) & S_{D_{\bar{p}}^{bu},eq,uv}(P_j, P_k, \omega) & S_{D_{\bar{p}}^{bu},eq,uw}(P_j, P_k, \omega) \\ S_{D_{\bar{p}}^{bu},eq,vu}(P_j, P_k, \omega) & S_{D_{\bar{p}}^{bu},eq,vv}(P_j, P_k, \omega) & S_{D_{\bar{p}}^{bu},eq,vw}(P_j, P_k, \omega) \\ S_{D_{\bar{p}}^{bu},eq,wu}(P_j, P_k, \omega) & S_{D_{\bar{p}}^{bu},eq,wv}(P_j, P_k, \omega) & S_{D_{\bar{p}}^{bu},eq,ww}(P_j, P_k, \omega) \end{bmatrix} \tag{16}$$

$$(j = 1, 2, \ldots, n; k = 1, 2, \ldots, n)$$

$$S_{D_{\bar{p}}^{bu},eq,ab}(P_j, P_k, \omega) = \bar{I}_{D_{\bar{p}}^{bu},a}(\omega)\bar{I}^{*}_{D_{\bar{p}}^{bu},b}(\omega)\sqrt{S_{ab}(P_j, \omega)S_{ab}(P_k, \omega)}\,R_{ab}(P_j, P_k, \omega) \quad (a = u, v, w\,;\, b = u, v, w) \tag{17}$$

where $\boldsymbol{S}_{D_{\bar{p}}^{bu},jk}(\omega)$ is the 3×3 matrix of the cross spectral density functions between three equivalent turbulent wind velocities at the center point (point j) of the jth element and the center point (point k) of the kth element; $R_{ab}(P_j, P_k, \omega)$ is the coherence function between turbulent wind components a and b at point j and point k; $S_{ab}(P_j, \omega)$ is the cross spectral density function between turbulent wind components a and b at the same point j; the product $\bar{I}_{D_{\bar{p}}^{bu},a}(\omega)\bar{I}^{*}_{D_{\bar{p}}^{bu},b}(\omega)$ is defined as aerodynamic admittance functions; $\bar{I}_{D_{\bar{p}}^{bu},a}(\omega)$ and $\bar{I}_{D_{\bar{p}}^{bu},b}(\omega)$ are, respectively, the Fourier transform of $I_{D_{\bar{p}}^{bu},a}(t)$ and $I_{D_{\bar{p}}^{bu},b}(t)$; and the superscript "*" denotes a complex conjugate operation.

The matrix $\boldsymbol{S}^{0}_{D_{\bar{p}}^{bu}}(\omega)$ can be decomposed into the following product with the Choleskey's method

$$\boldsymbol{S}^{0}_{D_{\bar{p}}^{bu}}(\omega) = \boldsymbol{H}_{D_{\bar{p}}^{bu}}(\omega)\boldsymbol{H}^{T^{*}}_{D_{\bar{p}}^{bu}}(\omega) \tag{18}$$

Based on the spectral representation method (Shinozuka and Deodatis 1991, Deodatis 1996), the equivalent turbulent wind velocities along the bridge deck, $\boldsymbol{f}_{D_{\bar{p}}^{bu}}(t)$, associated with the drag force can be simulated by the following series as $\bar{N}\to\infty$

$$f_{D_{\bar{p}}^{bu},j}(t) = \sqrt{2\Delta\omega}\sum_{m=1}^{j}\sum_{l=1}^{\bar{N}}\left|H_{D_{\bar{p}}^{bu},jk}(\omega_{ml})\right|\cos(\omega_{ml}t - \theta_{D_{\bar{p}}^{bu},jk}(\omega_{ml}) + \Phi_{ml}), \quad j = 1, 2, 3, ..., 3n \tag{19}$$

where $\Delta\omega = \omega_{up}/\bar{N}$ is the frequency increment; ω_{up} is an upper cutoff frequency beyond which the elements of the cross spectral density matrix $\boldsymbol{S}^{0}_{D_{\bar{p}}^{bu}}(\omega)$ are assumed to be zero; $H_{D_{\bar{p}}^{bu},jk}(\omega_{ml})$ is the element of $\boldsymbol{H}_{D_{\bar{p}}^{bu}}(\omega_{ml})$ at the jth row and kth column; $\theta_{D_{\bar{p}}^{bu},jk}(\omega_{ml}) = \tan^{-1}\{\mathrm{I_m}[H_{D_{\bar{p}}^{bu},jk}(\omega_{ml})]/\mathrm{R_e}[H_{D_{\bar{p}}^{bu},jk}(\omega_{ml})]\}$, which is the complex phase angle of $H_{D_{\bar{p}}^{bu},jk}(\omega_{ml})$; $\mathrm{I_m}[H_{jk}(\omega_{ml})]$ and $\mathrm{R_e}[H_{D_{\bar{p}}^{bu},jk}(\omega_{ml})]$ represent the imaginary and real parts of $H_{D_{\bar{p}}^{bu},jk}(\omega_{ml})$ respectively; $\Phi_{1l}, ..., \Phi_{jl}$, $l = 1, 2, ..., \bar{N}$ are the sequences of independent random phase angles distributed uniformly over the interval $[0, 2\pi]$; and ω_{ml} is of the double-indexing of the frequencies.

$$\omega_{ml} = (l - 1 + m/3n)\Delta\omega \qquad l = 1, 2, ..., \bar{N} \tag{20}$$

The application of the fast Fourier transform technique to the above algorithm can dramatically improve the computational efficiency for simulating the equivalent turbulent wind velocities $\boldsymbol{f}_{D_{\bar{p}}^{bu}}(t)$. The detail procedure of the fast Fourier transform technique is given in Deodatis (1996).

Clearly, the simulated time histories of equivalent turbulent wind velocities along the bridge deck associated with the drag force include not only the characteristics of incoming turbulent wind but also the aerodynamic admittance functions of bridge deck. The same procedure can be applied to generate the time histories of equivalent turbulent wind velocities along the bridge deck associated with other forces. Finally, the time histories of buffeting forces along the bridge deck can be obtained through Eqs. (5) to (7).

2.3. Self-excited forces due to skew winds

The self-excited forces acting on the bridge deck due to wind-structure interaction can be expressed as the function of mean wind speed $\overline{U}$, the aerodynamic impulse functions associated with the flutter derivatives measured under skew winds, and the bridge motion. By performing a series of coordinate transformations, the vector of self-excited forces acting on the bridge deck due to skew winds in the global structural coordinate system can be found as

$$\boldsymbol{F}^{se}(t) = \sum_{i=1}^{n} \boldsymbol{T}_i^{se} \overline{\boldsymbol{F}}_i^{se}(t) \tag{21}$$

where $\overline{\boldsymbol{F}}_i^{se}(t)$ is the 12×1 vector of self-excited forces at the nodes of the ith element of the bridge deck with respect to the global structural coordinate XYZ-system; and $\boldsymbol{T}_i^{se}(i = 1, ..., n)$ is the $N \times 12$ matrix with its elements being either zero or unit to locate the vector $\overline{\boldsymbol{F}}_i^{se}(t)$ at the proper position in the global vector $\boldsymbol{F}^{se}(t)$. The expression of $\overline{\boldsymbol{F}}_i^{se}(t)$ can be written as

$$\overline{\boldsymbol{F}}_i^{se}(t) = \overline{\boldsymbol{T}}_{GsLs,i} \tilde{\boldsymbol{N}}_i^T \boldsymbol{T}_{LsLr} \overline{\boldsymbol{P}}_i^{se}(t) \tag{22}$$

where $\overline{\boldsymbol{P}}_i^{se}(t)$ is the 6×1 vector of self-excited forces per unit length of the ith oblique element of the bridge deck with respect to the local reference coordinate qph-system; $\boldsymbol{T}_{Lslr,i}$ is the 6×6 transformation matrix from the local reference coordinate system qph to the local structural coordinate system xyz for the ith element. According to the coordinate systems of qph and xyz shown in Fig. 1(b), the matrix $\boldsymbol{T}_{Lslr,i}$ can be expressed as

$$\boldsymbol{T}_{LsLr,i} = \begin{bmatrix} \overline{\boldsymbol{T}}_{LsLr,i} & \boldsymbol{0} \\ \boldsymbol{0} & \overline{\boldsymbol{T}}_{LsLr,i} \end{bmatrix}; \quad \overline{\boldsymbol{T}}_{LsLr,i} = \begin{bmatrix} 1 & 0 & 0 \\ 0 & -1 & 0 \\ 0 & 0 & -1 \end{bmatrix} \tag{23}$$

The vector $\overline{\boldsymbol{P}}_i^{se}(t)$ includes six components

$$\overline{\boldsymbol{P}}_i^{se}(t) = \{C_{q,i}^{se}(t) \;\; D_{p,i}^{se}(t) \;\; L_{h,i}^{se}(t) \;\; M_{\alpha,i}^{se}(t) \;\; M_{\gamma,i}^{se}(t) \;\; M_{\phi,i}^{se}(t)\}^T \tag{24}$$

where $C_{q,i}^{se}(t)$, $D_{p,i}^{se}(t)$, $L_{h,i}^{se}(t)$, $M_{\alpha,i}^{se}$, $M_{\gamma,i}^{se}(t)$ and $M_{\phi,i}^{se}(t)$ are, respectively, the self-excited crosswind force, drag, lift, pitching moment, rolling moment and yawing moment on the ith oblique element of the bridge deck with respect to the local reference coordinate qph system. Generally, only the self-excited drag force $D_{p,i}^{se}(t)$, lift force $L_{h,i}^{se}(t)$ and pitching moment $M_{\alpha,i}^{se}(t)$ are regarded to be important to the buffeting response prediction of the bridge (Scanlan 1978, Jain, *et al*. 1996). Correspondingly, wind tunnel tests were performed to determine the flutter derivatives associated with these three forces under skew winds (Zhu 2002c), and the other three forces, $C_{q,i}^{se}(t)$, $M_{\gamma,i}^{se}(t)$ and $M_{\phi,i}^{se}(t)$ are omitted in this study.

The vector $\overline{\boldsymbol{P}}_i^{se}(t)$ is the function of the air density ρ, the element width B_i, the mean wind speed at the center of the element $\overline{U}_i$, the aerodynamic impulse functions associated with the flutter derivatives of the element under skew winds, and the structural motion at the center of the element. The resulting expression is as follows

$$\bar{\boldsymbol{P}}_i^{se}(t) = \begin{Bmatrix} 0 \\ D_{p,i}^{se}(t) \\ L_{h,i}^{se}(t) \\ M_{\alpha,i}^{se}(t) \\ 0 \\ 0 \end{Bmatrix} = \frac{\rho \bar{U}_i^2}{2} \begin{Bmatrix} 0 \\ \int_{-\infty}^{t} f_{D_{p,i}^{se}}(t-\tau)\delta_{p,i}^{ce}(\tau)d\tau + \int_{-\infty}^{t} f_{D_{h,i}^{se}}(t-\tau)\delta_{h,i}^{ce}(\tau)d\tau + B_i\int_{-\infty}^{t} f_{D_{\alpha,i}^{se}}(t-\tau)\delta_{\alpha,i}^{ce}(\tau)d\tau \\ \int_{-\infty}^{t} f_{L_{p,i}^{se}}(t-\tau)\delta_{p,i}^{ce}(\tau)d\tau + \int_{-\infty}^{t} f_{L_{h,i}^{se}}(t-\tau)\delta_{h,i}^{ce}(\tau)d\tau + B_i\int_{-\infty}^{t} f_{L_{\alpha,i}^{se}}(t-\tau)\delta_{\alpha,i}^{ce}(\tau)d\tau \\ B_i\int_{-\infty}^{t} f_{M_{p,i}^{se}}(t-\tau)\delta_{p,i}^{ce}(\tau)d\tau + B_i\int_{-\infty}^{t} f_{M_{h,i}^{se}}(t-\tau)\delta_{h,i}^{ce}(\tau)d\tau + B_i^2\int_{-\infty}^{t} f_{M_{\alpha,i}^{se}}(t-\tau)\delta_{\alpha,i}^{ce}(\tau)d\tau \\ 0 \\ 0 \end{Bmatrix} \tag{25}$$

where $\delta_{p,j}^{ce}(t)$ and $\delta_{h,i}^{ce}(t)$ are the transverse displacements along the axis p and the axis h, respectively, and $\delta_{\alpha,i}^{ce}(t)$ is the torsional displacement around the axis q at the center of the ith element with respect to the local reference coordinate system qph. These displacements with respect to the local reference coordinate system can be related to those at the nodes of the element with respect to the local structural coordinate system through the coordinate transformation and displacement interpolation function. $f_{D_{a,i}^{se}}(t)$, $f_{L_{a,i}^{se}}(t)$, and $f_{M_{a,i}^{se}}(t)(a = p, h, \alpha)$ are the aerodynamic impulse functions, which can be obtained from the experimentally measured flutter derivatives of the oblique element of the bridge deck using the rational function approximation approach. For example, $f_{M_{a,i}^{se}}(t)$ can be given by

$$f_{M_{\alpha,i}^{se}}(t) = c_{M_{\alpha,i}^{se},1}\delta_{\alpha,i}^{ce}(t) + \frac{B_i}{\bar{U}_i}c_{M_{\alpha,i}^{se},2}\dot{\delta}_{\alpha,i}^{ce}(t) + \sum_{k=3}^{m_{M_{\alpha,i}^{se}}} c_{M_{\alpha,i}^{se},k}\int_{-\infty}^{t} e^{-\frac{d_{M_{\alpha,i}^{se},k}\bar{U}_i}{B_i}(t-\tau)}\dot{\delta}_{\alpha,i}^{ce}(\tau)d\tau \tag{26}$$

where the value of $m_{M_{\alpha,i}^{se}}$ determines the level of accuracy of the approximation; $c_{M_{\alpha,i}^{se},i}$ and $d_{M_{\alpha,i}^{se},k}$ ($i = 1,2,\ldots, m_{M_{\alpha,i}^{se}}$; $k = 3,\ldots, m_{M_{\alpha,i}^{se}}$) are the dimensionless coefficients, which can be determined by the non-linear least-squares fit of the flutter derivatives A_2^* and A_3^* as follows (Bucher and Lin 1988).

$$A_3^*(V_i) = \frac{V_i^2 c_{M_{\alpha,i}^{se},1}}{4\pi^2} + \sum_{k=3}^{m_{M_{\alpha,i}^{se}}} \frac{V_i^2 c_{M_{\alpha,i}^{se},k}}{V_i^2 d_{M_{\alpha,i}^{se},k}^2 + 4\pi^2};\quad A_2^*(V_i) = \frac{V_i c_{M_{\alpha,i}^{se},2}}{2\pi} + \sum_{k=3}^{m_{M_{\alpha,i}^{se}}} \frac{V_i^3 c_{M_{\alpha,i}^{se},k}\, d_{M_{\alpha,i}^{se},k}}{V_i^2 d_{M_{\alpha,i}^{se},k}^2 + 8\pi^2} \tag{27}$$

in which $V_i = (2\pi\bar{U}_i)/(B_i\omega)$ is the reduced mean wind velocity.

The substitution of Eq. (26) to Eq. (25) then yields

$$\bar{\boldsymbol{P}}_i^{se}(t) = \begin{Bmatrix} 0 \\ D_{p,i}^{se}(t) \\ L_{h,i}^{se}(t) \\ M_{\alpha,i}^{se}(t) \\ 0 \\ 0 \end{Bmatrix} = \frac{\rho \bar{U}_i^2}{2} \boldsymbol{K}_i^{se} \begin{Bmatrix} 0 \\ \delta_{p,i}^{ce}(t) \\ \delta_{h,i}^{ce}(t) \\ \delta_{\alpha,i}^{ce}(t) \\ 0 \\ 0 \end{Bmatrix} + \frac{\rho \bar{U}_i B_i}{2} \boldsymbol{C}_i^{se} \begin{Bmatrix} 0 \\ \dot{\delta}_{p,i}^{ce}(t) \\ \dot{\delta}_{h,i}^{ce}(t) \\ \dot{\delta}_{\alpha,i}^{ce}(t) \\ 0 \\ 0 \end{Bmatrix} + \frac{\rho \bar{U}_i^2}{2} \bar{\boldsymbol{P}}_{lag,i}^{se}(t) \tag{28}$$

$$\boldsymbol{K}_i^{se} = \begin{bmatrix} 0 & 0 & 0 & 0 & 0 & 0 \\ 0 & c_{D_{p,i}^{se},1} & c_{D_{h,i}^{se},1} & B_i c_{D_{\alpha,i}^{se},1} & 0 & 0 \\ 0 & c_{L_{p,i}^{se},1} & c_{L_{h,i}^{se},1} & B_i c_{L_{\alpha,i}^{se},1} & 0 & 0 \\ 0 & B_i c_{M_{p,i}^{se},1} & B_i c_{M_{h,i}^{se},1} & B_i^2 c_{M_{\alpha,i}^{se},1} & 0 & 0 \\ 0 & 0 & 0 & 0 & 0 & 0 \\ 0 & 0 & 0 & 0 & 0 & 0 \end{bmatrix}; \boldsymbol{C}_i^{se} = \begin{bmatrix} 0 & 0 & 0 & 0 & 0 & 0 \\ 0 & c_{D_{p,i}^{se},2} & c_{D_{h,i}^{se},2} & B_i c_{D_{\alpha,i}^{se},2} & 0 & 0 \\ 0 & c_{L_{p,i}^{se},2} & c_{L_{h,i}^{se},2} & B_i c_{L_{\alpha,i}^{se},2} & 0 & 0 \\ 0 & B_i c_{M_{p,i}^{se},2} & B_i c_{M_{h,i}^{se},2} & B_i^2 c_{M_{\alpha,i}^{se},2} & 0 & 0 \\ 0 & 0 & 0 & 0 & 0 & 0 \\ 0 & 0 & 0 & 0 & 0 & 0 \end{bmatrix} \tag{29}$$

$$\bar{\boldsymbol{P}}_{lag,i}^{se}(t) = \begin{Bmatrix} 0 \\ \sum_{k=3}^{m_{D_{p,i}^{se}}} c_{D_{p,i}^{se},k} I_{D_{p,i}^{se},k}(t) + \sum_{k=3}^{m_{D_{h,i}^{se}}} c_{D_{h,i}^{se},k} I_{D_{h,i}^{se},k}(t) + B_i \sum_{k=3}^{m_{D_{\alpha,i}^{se}}} c_{D_{\alpha,i}^{se},k} I_{D_{\alpha,i}^{se},k}(t) \\ \sum_{k=3}^{m_{L_{p,i}^{se}}} c_{L_{p,i}^{se},k} I_{L_{p,i}^{se},k}(t) + \sum_{k=3}^{m_{L_{h,i}^{se}}} c_{L_{h,i}^{se},k} I_{L_{h,i}^{se},k}(t) + B_i \sum_{k=3}^{m_{L_{\alpha,i}^{se}}} c_{L_{\alpha,i}^{se},k} I_{L_{\alpha,i}^{se},k}(t) \\ B_i \sum_{k=3}^{m_{M_{p,i}^{se}}} c_{M_{p,i}^{se},k} I_{M_{p,i}^{se},k}(t) + B_i \sum_{k=3}^{m_{M_{h,i}^{se}}} c_{M_{h,i}^{se},k} I_{M_{h,i}^{se},k}(t) + B_i^2 \sum_{k=3}^{m_{M_{\alpha,i}^{se}}} c_{M_{\alpha,i}^{se},k} I_{M_{\alpha,i}^{se},k}(t) \\ 0 \\ 0 \end{Bmatrix} \tag{30}$$

where $I_{P_{a,i}^{se},k}(t)$ ($P_{a,i}^{se} = D_{p,i}^{se}, D_{h,i}^{se}, D_{\alpha,i}^{se}, L_{p,i}^{se}, L_{h,i}^{se}, L_{\alpha,i}^{se}, M_{p,i}^{se}, M_{h,i}^{se}, M_{\alpha,i}^{se}$; $k = 3, ..., m_{P_{a,i}^{se}}$) are the convolution integrations of the ith element, which can be calculated using a recursive algorithm. For instance, $I_{M_{\alpha,i}^{se},3}(t)$ can be computed by

$$I_{M_{\alpha,i}^{se},3}(t) = \int_{-\infty}^{t} e^{-\frac{d_{M_{\alpha,i}^{se},3}\bar{U}_i}{B_i}(t-\tau)} \dot{\delta}_{\alpha,i}^{ce}(t)\, d\tau \approx \frac{\Delta t}{2} \dot{\delta}_{\alpha,i}^{ce}(t) + e^{-\frac{d_{M_{\alpha,i}^{se},3}\bar{U}_i}{B_i}\Delta t} \left[I_{M_{\alpha,i}^{se},3}(t-\Delta t) + \frac{\Delta t}{2} \dot{\delta}_{\alpha,i}^{ce}(t-\Delta t) \right] \tag{31}$$

2.4. Step-by-step solution

In predicting the buffeting response of a long suspension bridge under skew winds, the Newmark's constant-average-acceleration scheme is used to find the step-by-step solution for the governing equation of motion of the bridge under skew winds (see Eq. (1)). The selection of the Newmark's constant-average-acceleration scheme is because of its unconditonal numerical stability compared with other schemes (Bathe 1982). Rewrite the governing equation of motion for the time step $t + \Delta t$.

$$\boldsymbol{M}^s\ddot{\boldsymbol{\Delta}}(t+\Delta t) + \boldsymbol{C}^s\dot{\boldsymbol{\Delta}}(t+\Delta t) + \boldsymbol{K}^s\Delta(t+\Delta t) = \boldsymbol{F}^{bu}(t+\Delta t) + \boldsymbol{F}^{se}(t+\Delta t) \tag{32}$$

where Δt is the time interval.

The formulations for the nodal displacement, velocity, and acceleration at time $t + \Delta t$ can be obtained as

$$\boldsymbol{\Delta}(t+\Delta t) = \tilde{\boldsymbol{K}}^{-1}\tilde{\boldsymbol{F}}(t+\Delta t) \tag{33}$$

$$\ddot{\boldsymbol{\Delta}}(t+\Delta t) = a_0(\boldsymbol{\Delta}(t+\Delta t) - \Delta(t)) - a_2\dot{\boldsymbol{\Delta}}(t) - a_3\ddot{\boldsymbol{\Delta}}(t) \tag{34}$$

$$\dot{\boldsymbol{\Delta}}(t+\Delta t) = \dot{\boldsymbol{\Delta}}(t) + a_6\ddot{\boldsymbol{\Delta}}(t) + a_7\ddot{\boldsymbol{\Delta}}(t+\Delta t) \tag{35}$$

where

$$\tilde{\boldsymbol{K}} = \boldsymbol{K}^s + a_0\boldsymbol{M}^s + a_1\boldsymbol{C}^s \tag{36}$$

$$\tilde{\boldsymbol{F}}(t+\Delta t)$$
$$= \boldsymbol{F}^{bu}(t+\Delta t) + \boldsymbol{F}^{se}(t+\Delta t) + \boldsymbol{M}^s(a_0\boldsymbol{\Delta}(t) + a_2\dot{\boldsymbol{\Delta}}(t) + a_3\ddot{\boldsymbol{\Delta}}(t)) + \boldsymbol{C}^s(a_1\boldsymbol{\Delta}(t) + a_4\dot{\boldsymbol{\Delta}}(t) + a_5\ddot{\boldsymbol{\Delta}}(t)) \tag{37}$$

in which $a_i (i = 0, 1, ..., 7)$ are the constant coefficients given by Bathe (1982).

$$a_0 = \frac{1}{\beta\Delta t^2};\quad a_1 = \frac{\gamma}{\beta\Delta t};\quad a_2 = \frac{1}{\beta\Delta t};\quad a_3 = \frac{1}{2\beta} - 1 \tag{38a-d}$$

$$a_4 = \frac{\gamma}{\beta} - 1;\quad a_5 = \left(\frac{\gamma}{\beta} - 2\right)\frac{\Delta t}{2};\quad a_6 = (1-\gamma)\Delta t;\quad a_7 = \gamma\Delta t \tag{38 e-h}$$

where γ and β are taken as 0.5 and 0.25 in this study. It is noted that the self-excited force vector on the bridge, $\boldsymbol{F}^{se}(t+\Delta t)$, in Eq. (37) is the function of bridge motion as shown in Eq. (28). Iterations should be performed in each time step. For instance, for the time step $t + \Delta t$, use the self-excited se force $\boldsymbol{F}^{se}(t)$ in the time step t to replace $\boldsymbol{F}^{se}(t+\Delta t)$ in Eq. (37) initially to compute the motion of the bridge deck. Then, use the computed bridge motion to calculate the self-excited forces again. Repeat the above two steps until the bridge motion is converged to the prescribed criteria.

3. Tsing Ma suspension bridge and Typhoon Sam

3.1. Tsing Ma bridge and WASHMS

The Tsing Ma Bridge in Hong Kong is a long suspension bridge carrying a dual three-lane highway on the upper level of the bridge deck and two railway tracks and two carriageways on the lower level within the bridge deck. The alignment of the bridge deck deviates from the east-west axis for about 17° in anti-clockwise. The typical section of the bridge deck is 41 m wide and 7.643 m high. The two bridge towers of 206 m high are made of pre-stressed concrete. The east bridge tower sits on the northwest shoreline of Tsing Yi Island, called the Tsing Yi tower while the west bridge tower sits on Ma Wan Island, called the Ma Wan tower (see Fig. 2).

To monitor the health status of the Tsing Ma Bridge, an instrumentation system called the Wind And Structural Health Monitoring System (WASHMS) was installed in the bridge by the Hong

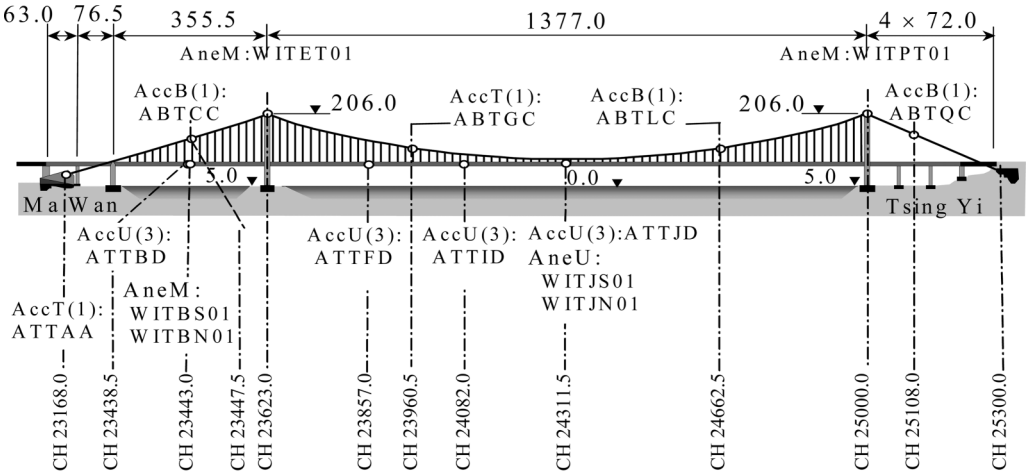

Fig. 2 Locations of anemometers and accelerometers

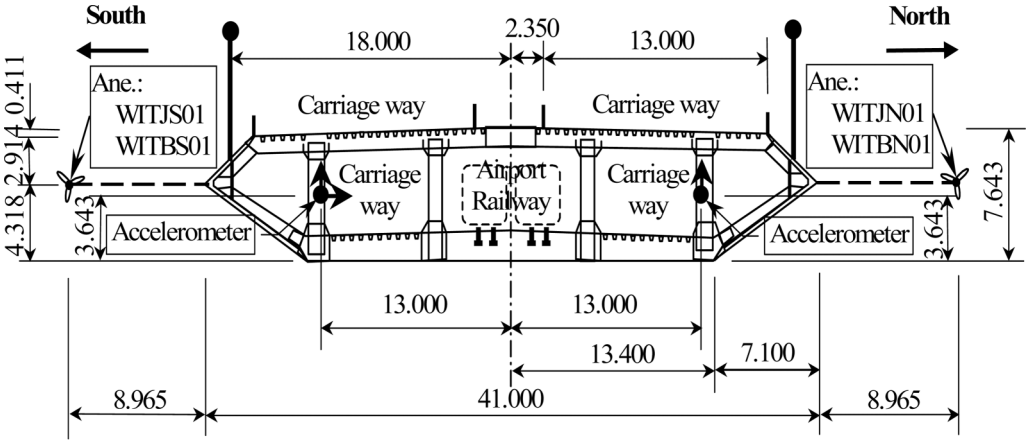

Fig. 3 Positions of sensors on cross section of bridge deck

Kong Highways Department (Lau, *et al.* 1998). The WASHMS has seven types of sensors including six sets of anemometer and 24 uni-axial servo type accelerometers. Two digital ultrasonic anemometers (AneU) were installed on the north side and south side, respectively, of the bridge deck at the middle main span (75.314 m in elevation). They are specified as WITJN01 and WITJS01 in Figs. 2 and 3. Two analogue mechanical anemometers (AneM) were located at two sides of the bridge deck near the middle of the Ma Wan side span (62.944 m in elevation), specified as WITBN01 at the north side and WITBS01 at the south side in Figs. 2 and 3. Another two analogue mechanical anemometers (AneM) were arranged over the top of each bridge tower (217.084 m in elevation). They are specified as WITPT01 for the Tsing Yi tower and WITET01 for the Ma Wan tower.

A total of 12 uni-axial accelerometers were used in AccU measurement, which was arranged at the four deck sections ATTID, ATTJD, ATTFD and ATTBD (see Fig. 2). AccU means the uni-axial measurement by using only one accelerometer to give signal in one prescribed direction. It is see from Fig. 3 that at each section, there are two accelerometers, horizontally separated with 13 m, measuring acceleration in the vertical direction and one accelerometer measuring acceleration in the lateral direction.

3.2. Typhoon Sam and wind characteristics

After developed at about 680 km east-northeast of Manila on 19 August 1999, the tropical depression Sam moved west-northeast wards over the Pacific and intensified into a tropical storm at that night. It then moved north-westly towards the coast of Guangdong and became a typhoon on a late morning of 22 August near Hong Kong. Typhoon Sam finally made landfall over the eastern part of Sai Kung in Hong Kong at around 6 p.m. on 22 August. Following landfall, Sam traversed the northeastern part of the New Territories at a speed of about 25 km/h and crossed into Shenzhen, and then weakened gradually over inland Guangdong on 23 August. The WASHMS timely recorded wind velocity and bridge buffeting responses. The sampling frequency for wind velocity was 2.56 Hz and the cutoff frequency was 1.28 Hz. The sampling frequency of acceleration response was 25.6 Hz and the cutoff frequncy was 12.8 Hz.

After a careful examination of all the measured wind velocity time histories, one-hour record of wind velocity between 14:11 to 15:11 Hong Kong Time (HKT) on 22 August 1999 was selected for the analysis. During this period, incident wind blew to the Tsing Ma Bridge from the direction near to the north. Therefore, the wind data recorded by the anemometers installed at the south side of the bridge deck were contaminated by the bridge deck itself and were not suitable for the analysis of natural wind structures. Due to the technical reason, the mechanical anemometers installed at the deck and the top of the towers failed to record the wind azimuth. As a result, wind characteristics of Typhoon Sam surrounding the bridge could be extracted only from the wind speed histories recorded by the three-component ultrasonic anemometer installed on the north side of the bridge deck at the mid-span. By analyzing the three-components of the recorded wind velocity, it was found that the hourly-mean wind speed was about 17.1 m/s and the mean wind blew from north-northeast. The global hourly-mean wind yaw angle β_0 and inclination θ_0 were, respectively, -29.15^o and 2.25^o. The time histories of fluctuating wind speeds $u(t)$, $v(t)$ and $w(t)$ in the longitudinal (along-wind), lateral, and upward directions were also extracted from the measured three components of wind velocity, respectively. It was found that the turbulence intensities were about 18.6%, 20.4% and 14.5%, for $u(t)$, $v(t)$ and $w(t)$, respectively, and the corresponding integral scales of turbulence were 228 m, 116 m, and 84 m based on the Taylor's hypothesis.

The spectral analysis was performed on the measured three fluctuating wind speeds $u(t)$, $v(t)$ and

$w(t)$ with the hamming window and the piecewise smoothing method. A general objective function of four parameters for wind spectrum was used to fit the measured normalized auto and cross spectra of wind turbulence by minimizing the residue function via non-linear least squares fitting technique (Zhu 2002a). The one-side three auto spectra obtained from this exercise were given as

$$\frac{nS_{uu}(n)}{u_*^2} = \frac{44.65f}{\left(1 + 18.71f^{\frac{1}{0.9997}}\right)^{\frac{c}{0.9997}}} \tag{39a}$$

$$\frac{nS_{vv}(n)}{u_*^2} = \frac{30.44f}{\left(1 + 11.25f^{\frac{1}{0.9873}}\right)^{\frac{c}{0.9873}}} \tag{39b}$$

$$\frac{nS_{ww}(n)}{u_*^2} = \frac{9.573f}{\left(1 + 51.74f^{\frac{1}{0.5608}}\right)^{\frac{c}{0.5608}}} \tag{39c}$$

where c is the constant of 5/3; n is the frequency in Hz; $f = nz / \overline{U}(z)$ is the non-dimensional reduced frequency; z is the height above the sea level; and u_* is the friction velocity, estimated as 1.69 m/s from the measured horizontal shear stress.

The one-side co-spectra between every two of the three fluctuating wind speeds were given as

$$\frac{nS_{uv}(n)}{u_*^2} = \frac{-19.24f}{\left(1 + 46.65f^{\frac{1}{0.70}}\right)^{\frac{2.4}{0.70}}} \tag{40a}$$

$$\frac{nS_{uw}(n)}{u_*^2} = \frac{-8.66f}{\left(1 + 56.93f^{\frac{1}{0.59}}\right)^{\frac{2.4}{0.59}}} \tag{40b}$$

$$\frac{nS_{vw}(n)}{u_*^2} = \frac{2.08f}{\left(1 + 13.33f^{\frac{1}{0.56}}\right)^{\frac{2.4}{0.56}}} \tag{40c}$$

The quadrature spectra between every two of the three fluctuating wind speeds were insignificant and neglected in this study. The coherence function used in the study is taken the form as

$$R_{ab}(P_j, P_k, n) = \exp(-\hat{f}_{ab}(P_j, P_k, n)) \quad (a = u, v, w\ ;\ b = u, v, w) \tag{41a}$$

$$\hat{f}_{aa}(P_j, P_k, n) = \frac{n\sqrt{[C^a_{X_u}(X_{u,j} - X_{u,k})]^2 + [C^a_{Y_u}(Y_{v,j} - Y_{v,k})]^2 + [C^a_{Z_w}(Z_{w,j} - Z_{w,k})]^2}}{(\overline{U}_j + \overline{U}_k)/2} \tag{41b}$$

$$\hat{f}_{ab}(P_j, P_k, n) = \frac{\hat{f}_{aa}(P_j, P_k, n) + \hat{f}_{bb}(P_j, P_k, n)}{2} \tag{41c}$$

where $X_{u,i}$, $Y_{v,i}$ and $Z_{w,i}$ are the coordinates of spatial points $P_i(i = j, k)$ in the global wind coordinate $X_uY_vZ_w$-system; $\overline{U}_i(i = j, k)$ is the mean wind velocity at the point $P_i(i = j, k)$; $C^a_{X_u}$, $C^a_{Y_v}$ and $C^a_{Z_w}(a = u, v, w)$ are the exponential decay coefficients, taken as $C^u_{X_u} = 3.0$, $C^v_{X_u} = 3.0$, $C^w_{X_u} = 3.0$, $C^u_{Y_v} = 16.0$, $C^v_{Y_v} = 11.0$, $C^w_{Y_v} = 8.0$, $C^u_{Z_w} = 10.0$, $C^v_{Z_w} = 7.0$, and $C^w_{Z_w} = 7.0$ in this study.

3.3. Measured bridge deck acceleration responses

To be consistent with wind characteristics analysis, only the acceleration response data recorded from 14:11 to 15:11 HKT on 22 August 1999 were analysed. They include the lateral, vertical and torsional accelerations at the three deck sections in the main span (ATTJD, ATTID and ATTFD) and one deck section in the Ma Wan side span (ATTBD). The root mean square (RMS) acceleration responses of the bridge deck at the four deck sections (ATTJD, ATTID, ATTFD and ATTBD) are plotted in Fig. 10 to compare with the computed results.

4. Comparison between computed and measured buffeting responses

A computer program was written for the time domain buffeting analysis of long suspension bridges under skew winds based on the formulae derived in Section 2. The computer program is now used to perform the buffeting analysis of the Tsing Ma suspension bridge under skew winds during Typhoon Sam between 14:11 to 15:11 HKT on 22 August 1999. The computed buffeting responses are then compared with the field measurement results.

4.1. The bridge model

The three-dimensional dynamic finite element model of the Tsing Ma suspension Bridge has been established and updated by Xu, *et al*. (1997) using the dynamic properties from the ambient vibration measurement. Three-dimensional Timoshenko beam elements with rigid arms were used to model the two bridge towers. The cables and suspenders were modelled by cable elements accounting for geometric nonlinearity due to cable tension. The hybrid steel bridge deck was represented by a single beam with equivalent cross-sectional properties determined from a finite element analysis using detailed sectional modes. The connections between bridge components and the supports of the bridge were properly modelled. The first 150 natural frequencies range from 0.068 to 2.008 Hz. Fig. 4 shows the first two modes of vibration in vertical, lateral and torsional directions, respectively.

To constitute the damping matrix of the bridge, the Rayleigh damping assumption is used in this study. The two modal damping ratios of the bridge of 1% each, measured from the first symmetric lateral and vertical modes of the main span of the bridge deck, are used to form the damping matrix. The corresponding natural frequencies of the bridge are 0.068 Hz and 0.210 Hz, respectively, in the first symmetric lateral and vertical modes of vibration.

4.2. Aerodynamic properties of an oblique strip of bridge deck

To carry out the comparison of buffeting response of the Tsing Ma suspension bridge under skew winds between field measurement and analysis, the aerodynamic coefficients and flutter derivatives

Frequency	Mode shape
First Vertical Mode f_{V1}=0.117Hz	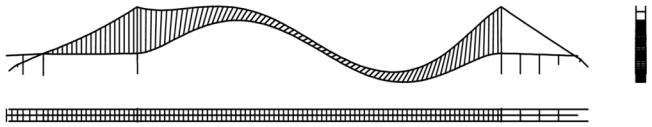
Second Vertical Mode f_{V2}=0.137Hz	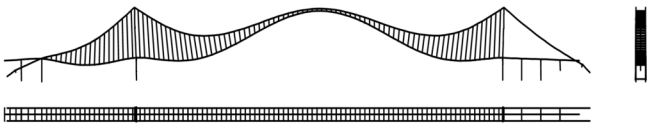
First Lateral Mode f_{L1}=0.068 Hz	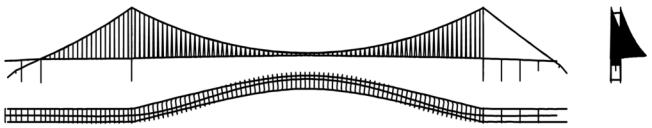
Second Lateral Mode f_{L2}=0.158 Hz	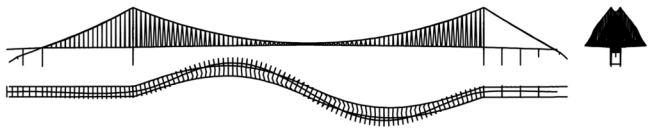
First Torsional Mode f_{T1}=0.271Hz	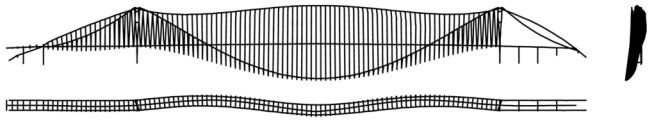
Second Torsional Mode f_{T2}=0.311Hz	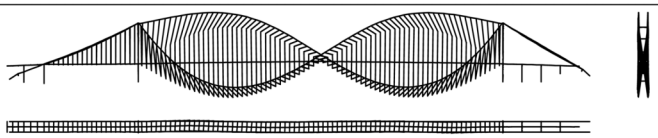

Fig. 4 First two modes of vibration of Tsing Ma Bridge in vertical, lateral and torsional directions

of the bridge deck under skew winds were measured through wind tunnel tests by Zhu, *et al*. (2002b, 2002c). The measured aerodynamic coefficients and their derivatives with respect to wind inclination and yaw angle (β_0 = -29.15°, θ_0 = 2.25°) of a typical oblique strip of the bridge deck under skew wind are listed in Table 1 and used in the simulation of buffeting forces.

The measured eight flutter derivatives of H_i^* and A_i^* (i = 1,2,3,4) of the oblique strip of the bridge deck under skew wind (β_0 = -29.15°, θ_0 = 2.25°) as a function of reduced velocity are fitted by the rational functions (see Eq. (27)) for the determination of self-excited forces. The measured flutter derivatives and the fitting curves are shown in Fig. 5 and the resulting dimensional coefficients are listed in Table 2. The flutter derivatives P_1^* and P_3^* are not available from the wind tunnel tests. The formulae based on the quasi-steady theory were thus employed and fitted by the rational functions. All other flutter derivatives were considered insignificant to the bridge buffeting

Table 1 Aerodynamic force coefficients of oblique strip of bridge deck (β_0 = -29.15°, θ_0 = 2.25°) (Zhu 2002b)

$C_{C_{\bar{q}}}$	$C_{D_{\bar{p}}}$	$C_{L_{\bar{h}}}$	$C_{M_{\bar{\alpha}}}$	$C_{M_{\bar{\gamma}}}$	$C_{M_{\bar{\phi}}}$
-0.0237	0.0794	0.0801	-0.0660	-0.0011	-0.0307
$C'^{\bar{\beta}}_{C_{\bar{q}}}$	$C'^{\bar{\beta}}_{D_{\bar{p}}}$	$C'^{\bar{\beta}}_{L_{\bar{h}}}$	$C'^{\bar{\beta}}_{M_{\bar{\alpha}}}$	$C'^{\bar{\beta}}_{M_{\bar{\gamma}}}$	$C'^{\bar{\beta}}_{M_{\bar{\phi}}}$
0.0201	0.0607	-0.0811	-0.0377	-0.0228	0.0371
$C'^{\bar{\theta}}_{C_{\bar{q}}}$	$C'^{\bar{\theta}}_{D_{\bar{p}}}$	$C'^{\bar{\theta}}_{L_{\bar{h}}}$	$C'^{\bar{\theta}}_{M_{\bar{\alpha}}}$	$C'^{\bar{\theta}}_{M_{\bar{\gamma}}}$	$C'^{\bar{\theta}}_{M_{\bar{\phi}}}$
0.1712	-0.0313	2.6474	-0.5450	0.1145	0.0948

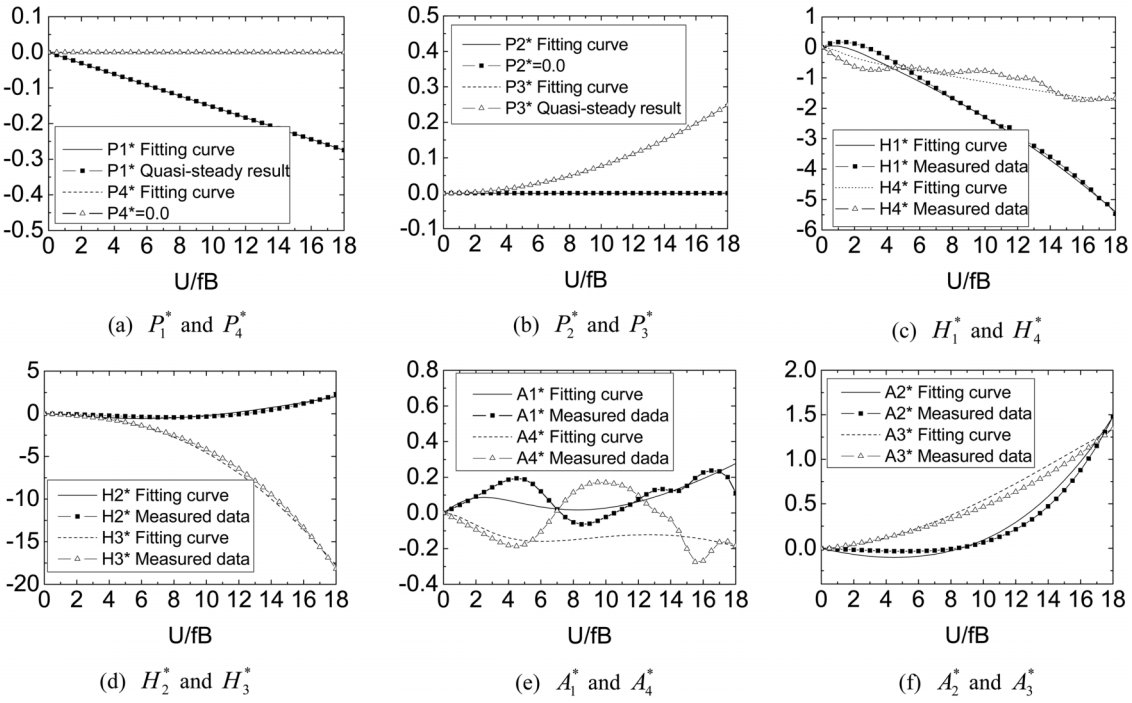

(a) P_1^* and P_4^* (b) P_2^* and P_3^* (c) H_1^* and H_4^*

(d) H_2^* and H_3^* (e) A_1^* and A_4^* (f) A_2^* and A_3^*

Fig. 5 Measured flutter derivatives versus rational function approximations

response and neglected in the computation. It is seen from Fig. 5 that except for A_1^* and A_4^*, all the concerned flutter derivatives can be well fitted. However, the measured flutter derivatives A_1^* and A_4^* oscillate so irregularly that they cannot be fitted properly.

There are no measurement data available on the aerodynamic admittance functions of the Tsing Ma bridge deck. The aerodynamic admittance function proposed by Davenport (1962) is employed for the 9 aerodynamic admittance functions associated with the buffeting drag, crosswind force, and yawing moment of the bridge deck.

Table 2 Coefficients of rational functions of oblique strip of bridge deck (β_0 = -29.15°, θ_0 = 2.25°)

	$P_a^{se} = D_p^{se}$	$P_a^{se} = D_\alpha^{se}$	$P_a^{se} = L_h^{se}$	$P_a^{se} = L_\alpha^{se}$	$P_a^{se} = M_h^{se}$	$P_a^{se} = M_\alpha^{se}$
$c_{P_a^{se},1}$	-0.0001	0.0303	0.2827	-1.9181	-0.0639	-0.9046
$c_{P_a^{se},2}$	-0.0924	0.0000	0.7103	-0.8908	0.4210	-0.2415
$c_{P_a^{se},3}$	-0.1982	0.0760	-5.7327	-2.2933	-0.8920	0.1605
$c_{P_a^{se},4}$	0.1661	-0.0760	-0.9180	-0.8439	-0.2929	1.1088
$c_{P_a^{se},5}$	0.0	0.0	-0.5231	3.2382	0.1661	0.0
$d_{P_a^{se},3}$	3.9003	1.5000	3.6314	0.7516	1.6889	1.4665
$d_{P_a^{se},4}$	3.4999	1.5000	2.0643	0.0261	5.2595	0.0753
$d_{P_a^{se},5}$	0.0	0.0	0.1746	0.5261	0.3669	0.0

Note: (1) $c_{P_a^{se},1} = c_{P_a^{se},2} = 0.0$ for $P_a^{se} = D_h^{se}, L_p^{se}, M_p^{se}$ in Eq. (29)
(2) $m_{P_a^{se}} = 5$ for $P_a^{se} = D_p^{se}, D_\alpha^{se}, L_h^{se}, L_\alpha^{se}, M_h^{se}, M_\alpha^{se}$ and $m_{P_a^{se}} = 0$ for $P_a^{se} = D_h^{se}, L_p^{se}, M_p^{se}$ in Eq. (30).

$$\overline{I}_{C_{\tilde{q}}^{bu,a}}(n)\overline{I}^{*}_{C_{\tilde{q}}^{bu,b}}(n) = \overline{I}_{D_{\tilde{p}}^{bu,a}}(n)\overline{I}^{*}_{D_{\tilde{p}}^{bu,b}}(n) = \overline{I}_{M_{\tilde{\phi}}^{bu,a}}(n)\overline{I}^{*}_{M_{\tilde{\phi}}^{bu,b}}(n) = \left|\chi_D(n)\right|^2 \quad (a = u, v, w; b = u, v, w) \tag{42}$$

$$\left|\chi_D(n)\right|^2 = 2(c - 1 + e^{-c})/c^2, \quad c = \lambda n D/\overline{U} \tag{43}$$

where the decay factor λ is set to 7; and D is taken as the height of the bridge deck of 7.643 m.

The other 9 aerodynamic admittance functions associated with the buffeting lift force, pitching moment, and rolling moment of the bridge deck are set to unity, namely

$$\overline{I}_{L_{\tilde{h}}^{bu,a}}(n)\overline{I}^{*}_{L_{\tilde{h}}^{bu,b}}(n) = \overline{I}_{M_{\tilde{\alpha}}^{bu,a}}(n)\overline{I}^{*}_{M_{\tilde{\alpha}}^{bu,b}}(n) = \overline{I}_{M_{\tilde{\gamma}}^{bu,a}}(n)\overline{I}^{*}_{M_{\tilde{\gamma}}^{bu,b}}(n) = 1.0 \ (a = u, v, w; b = u, v, w) \tag{44}$$

The above assumptions on the aerodynamic admittance functions were found suitable for the frequency domain buffeting analysis of the Tsing Ma suspension bridge (Zhu 2002a).

4.3. Simulation of equivalent turbulent wind velocities

Based on the concept of equivalent turbulent wind velocities described in Section 2, only two sets of equivalent turbulent wind velocities need to be simulated according to the aerodynamic admittance functions used for the Tsing Ma Bridge. One set of equivalent turbulent wind velocities is used for simulating the buffeting lift force, pitching moment, and rolling moment acting on the bridge deck, in which the aerodynamic admittance functions are set to unity and the spectra of the equivalent turbulent wind velocities are actually equal to the measured wind spectra from Typhoon Sam for a given position. Another set of equivalent turbulent wind velocities is used for simulating

the buffeting drag force, crosswind force, and yawing moment on the bridge deck, in which the spectra of the equivalent turbulent wind velocities are the measured wind spectra from Typhoon Sam times the Davenport's aerodynamic admittance functions for a given position. The measured auto spectra expressed by Eq. (39) and the co-spectra expressed by Eq. (40) are assumed to be the same for all the points along the bridge deck and used in the simulation of buffeting forces. Thus, the two sets of equivalent turbulent wind velocities to be simulated both are three-dimensional multivariate stochastic processes. It is noted that the two sets of equivalent turbulent wind velocities are respective to the global wind coordinate $X_uY_vZ_w$-system. Therefore, in the simulation the coordinate vector of each point on the bridge deck with respect to the global structural coordinate XYZ-system should be transformed to the global mean wind coordinate $X_uY_vZ_w$-system through the transformation matrix $\boldsymbol{T}_{GwGs}$, which is given by

$$\boldsymbol{T}_{GwGs} = \begin{bmatrix} -\cos\theta_0\sin\beta_0 & \cos\theta_0\cos\beta_0 & \sin\theta_0 \\ -\cos\beta_0 & -\sin\beta_0 & 0 \\ \sin\theta_0\sin\beta_0 & -\sin\theta_0\cos\beta_0 & \cos\theta_0 \end{bmatrix} \tag{45}$$

The time interval and duration used in the simulation are 0.0625s and 3600s, respectively. The variation of the bridge deck elevation between 58.73 m and 75.31 m is also taken into consideration via the mean wind speed profile of a power law. The total number of points along the bridge deck in the simulation N is 119. The upper cutoff frequency ω_{up} is 4π and the frequency increment $\Delta\omega$ is $4\pi/1024$. Therefore, about 150 modes of vibration of the bridge are naturally included in the time domain buffeting analysis. The major parameters used in the simulation and the time domain analysis are summarized in Table 3 for easy reference. The two sets of equivalent turbulent wind velocities are generated with the same independent random phase angles distributed uniformly over the interval $[0, 2\pi]$ so that all the buffeting forces can be regarded to simulate simultaneously. The time histories of the simulated three-dimensional turbulent velocity at point ATTJD are shown in Figs. 6 and 7, respectively, for the first and second sets of equivalent turbulent wind velocities. To examine the accuracy of the simulated results, the auto spectra and cross spectra of the simulated equivalent wind velocities at point ATTJD are computed using the time histories plotted in Fig. 7 for the second set of equivalent turbulent wind velocities and compared with the targeted auto

Table 3 Major parameters used in the simulation and the time domain analysis

Major Parameters	Values
Mean wind speed at the deck level	17.1 m/s
Power law of mean wind speed profile	$\alpha = 0.33$
Mean wind yaw angle and inclination	$\beta_0 = -29.15^o$, $\theta_o = 2.25^o$
Total number of simulation points along the bridge deck	$N = 119$
Longitudinal, lateral, and vertical turbulent intensities	18.6%, 20.4%, 14.5%
Upper cutoff frequency	$\omega_{up} = 4\pi$ rad/s
Frequency points	$N = 1024$
Frequency interval	$\Delta\omega = 0.012$ rad/s
Time interval	$\Delta t = 0.0625$s
Time duration	3600s

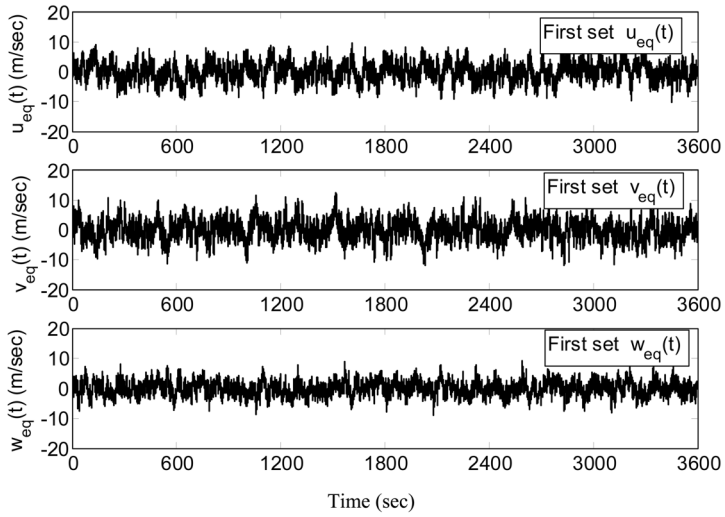

Fig. 6 The first set of equivalent fluctuating wind velocities at point ATTJD

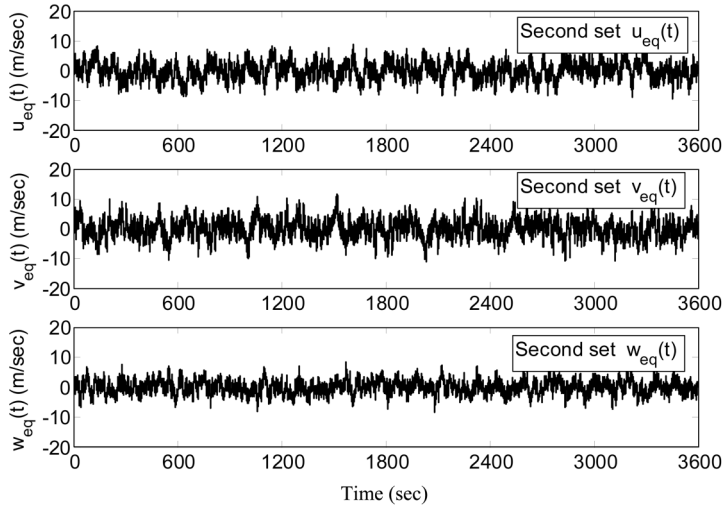

Fig. 7 The second set of equivalent fluctuating wind velocities at point ATTJD

spectra and cross spectra $|\chi_D(\omega)|^2 S_{ab}(\omega)(a = u, v, w;\ b = u, v, w)$, expressed by Eqs. (39),(40), and (43). The comparison is shown in Fig. 8, and it is seen that the simulated auto spectra and cross spectra match quite well to their respective targeted auto spectra and cross spectra.

4.4. Comparison of acceleration response of bridge deck

The time histories of lateral, vertical, and torsional acceleration responses of the Tsing Ma suspension bridge deck at the mid-main span (point ATTJD) under skew winds during Typhoon Sam from 14:11 to 15:11 HKT on 22 August 1999 are computed and displayed in Fig. 9. It is seen that the vertical acceleration response is much larger than the lateral acceleration response of the

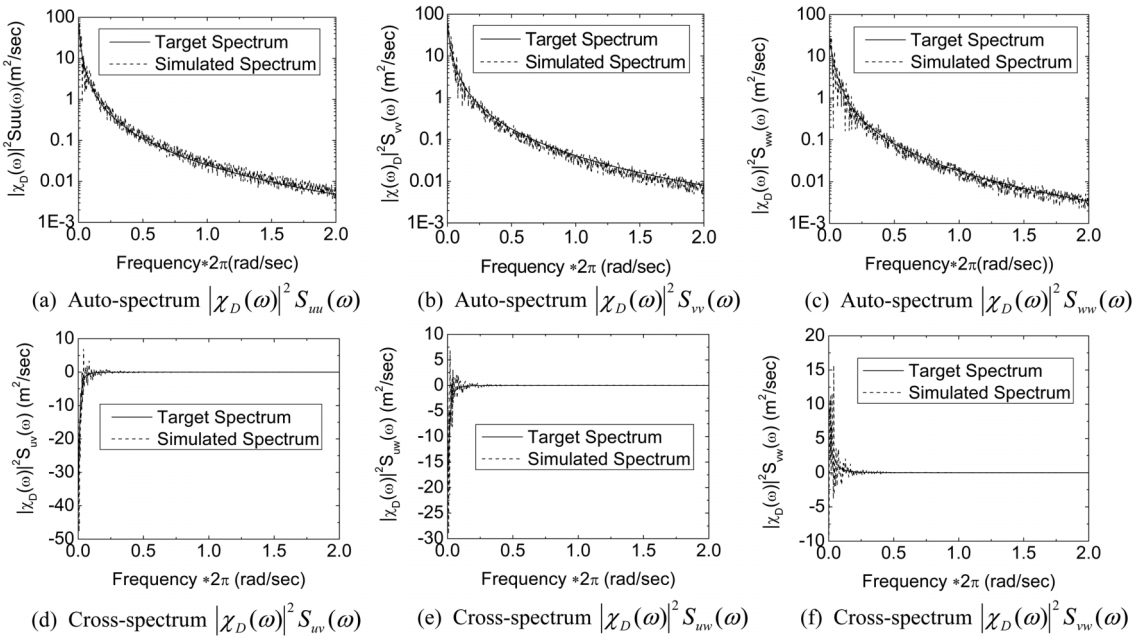

Fig. 8 Auto/cross spectra of equivalent fluctuating wind velocities versus targeted spectra

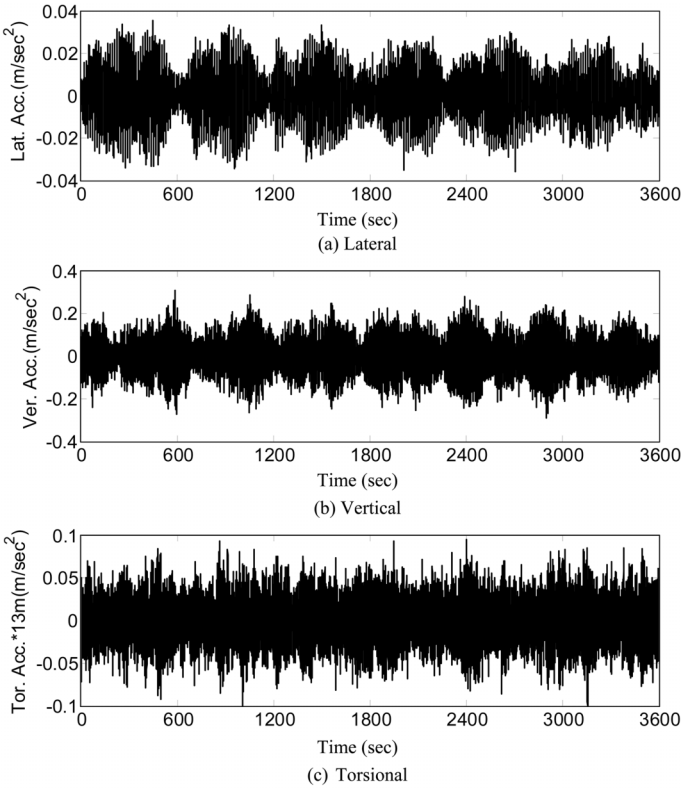

Fig. 9 Time histories of acceleration responses of bridge deck at point ATTJD

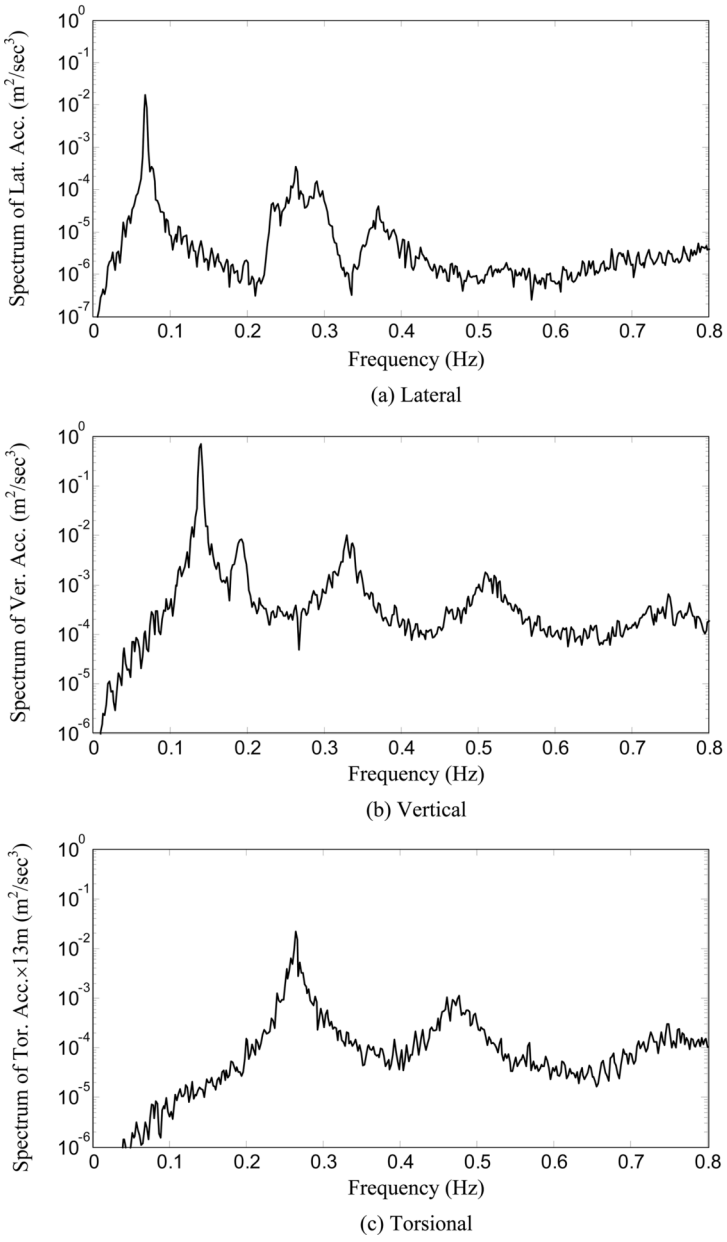

Fig. 10 Acceleration response spectra of bridge deck at point ATTJD

bridge deck at point ATTJD. Since point ATTJD is at the mid-span of the bridge deck, the acceleration responses are mainly attributed to the first a few symmetric modes of vibration in each direction.

Fig. 10 depicts the spectra of lateral, vertical, and torsional acceleration responses shown in Fig. 9. It is seen that the lateral acceleration response at point ATTJD is dominated by the first lateral symmetric mode of the bridge main span with a natural frequency of 0.068 Hz. The second

dominant spectral peak locates at a frequency of 0.271 Hz, which is the natural frequency of the first torsional symmetric mode of the bridge main span. The coupling effect between the lateral and torsional vibrations increases the lateral acceleration response. Furthermore, the second, third and fourth lateral symmetric modes of the bridge main span with natural frequencies of 0.232 Hz, 0.285 Hz and 0.365 Hz, respectively, also make moderate contributions to the total lateral acceleration response.

Similar observation can be made for the vertical acceleration at point ATTJD. The vertical

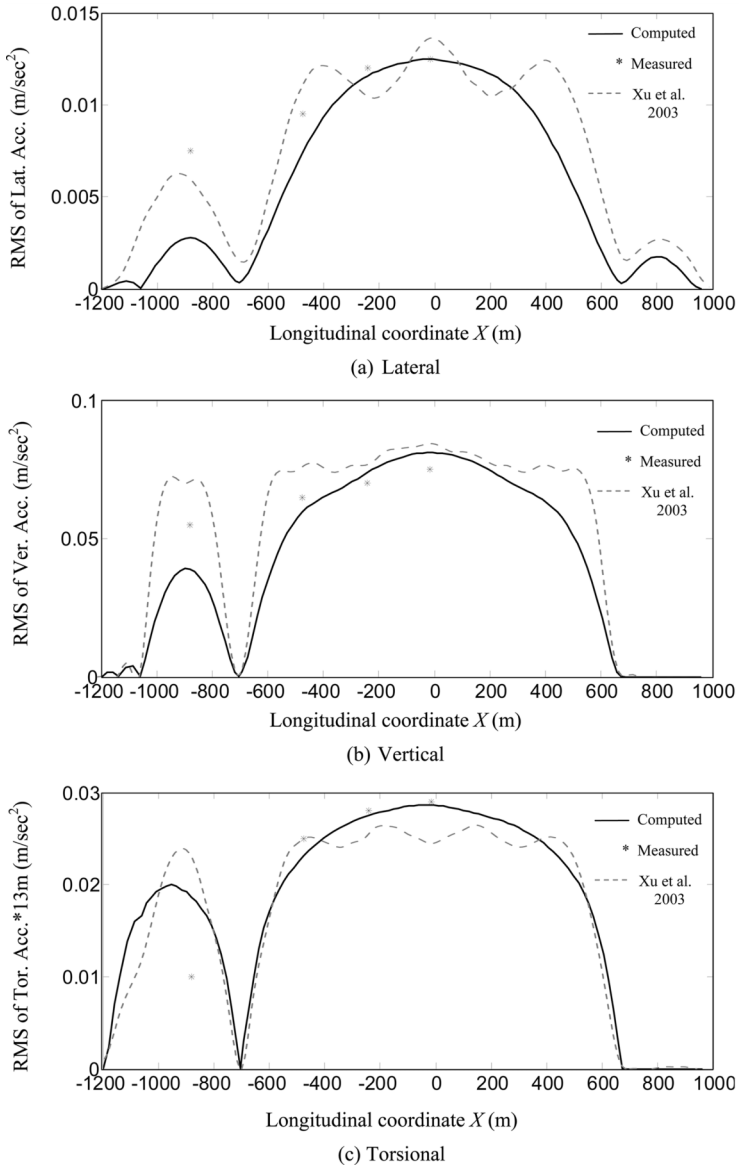

Fig. 11 Comparison between measured and computed deck RMS acceleration responses

acceleration response at point ATTJD is dominated by the first vertical symmetric mode of the bridge main span with a natural frequency of 0.137 Hz. The second and third vertical symmetric modes of the bridge main span with natural frequencies equal to 0.189 Hz and 0.325 Hz, respectively, have moderate effects on the total vertical acceleration response. The contribution from the further higher vertical symmetric modes of vibration is small. The torsional acceleration response at point ATTJD is dominated by the first torsional symmetric mode of the bridge main span with a natural frequency of 0.271 Hz. The second torsional symmetric mode of the bridge main span with a natural frequency of 0.4755 Hz has a moderate effect on the total torsional acceleration response.

The root mean square (RMS) acceleration responses of the bridge deck computed from the response time histories are plotted in Fig. 11 together with the measured RMS acceleration responses at the four specified deck sections in the lateral, vertical, and torsional directions, respectively. It is seen that for the main span, the computed RMS acceleration responses of the bridge deck in the lateral, vertical, and torsional directions are close to the measured results. By taking the measured results at the three points ATTFD, ATTID and ATTJD as references, the relative differences between the computed and measured results are -19.72%, -3.31% and -0.28%, respectively, for the lateral RMS acceleration responses; -7.57%, 6.25% and 8.22%, respectively, for the vertical RMS acceleration responses; and -7.37%, -1.89% and -1.10%, respectively, for the torsional RMS acceleration responses. For the Ma Wan side span, the computed RMS acceleration response in the vertical direction deviates from the measured one at point ATTBD, and the relative difference is -30.45%. In the lateral and torsional directions, the relative differences between the computed and measured RMS acceleration responses reach -63.16% and 45.71%, respectively.

The RMS acceleration responses of the bridge deck in the lateral, vertical, and torsional directions, obtained by using the frequency domain method (Xu, *et al*. 2003), are also plotted in Fig. 11. The buffeting forces on the bridge deck, the bridge towers and the main cables and their interactions were taken into consideration in the frequency domain analysis. It is seen that the time domain solutions are close to the frequency domain solutions for the bridge main span. However, the frequency domain solutions appear to contain the effects from the main cables, which are not considered in the time domain analysis. Furthermore, the time domain results are significantly smaller than the frequency domain results for the Ma Wan side span. This may be attributed to buffeting forces on the bridge towers and cables, which were taken into consideration in the frequency domain analysis but not in the time domain analysis. The inclusion of the interaction between the three major bridge components in the time domain analysis deserves to be considered in the future work.

5. Conclusions

A time domain approach for predicting the buffeting response of long suspension bridges under skew winds has been proposed in this study. The time histories of buffeting forces of six components along the bridge deck under skew winds are simulated in terms of the aerodynamic coefficients of an oblique deck strip measured under skew winds, the equivalent fluctuating wind velocities with aerodynamic impulse functions included, and the spectral representation method. The self-excited forces on the bridge deck are represented by the convolution integrals involving structural motions and aerodynamic impulse functions derived from experimentally measured flutter derivatives under skew winds.

Wind structures and buffeting responses measured by the Wind and Structural Health Monitoring System installed on the Tsing Ma suspension Bridge in Hong Kong during Typhoon Sam were analyzed. The proposed time domain approach was then applied to the Tsing Ma suspension bridge to compute its buffeting response caused by skew winds during Typhoon Sam and to compare the computed responses with the measured results and those computed by the frequency domain approach. The comparisons were found satisfactory in general for the bridge response in the main span but not for the bridge response in side spans.

It should be pointed out that in this study, the buffeting forces on the main cables and towers of the bridge were not included in this analysis because it was very time-consuming with the current spectral representation method to simulate a complete three-dimensional turbulent wind velocity field to cover not only the bridge deck but also the main cables and bridges towers. The inclusion of the interaction between the three major bridge components in the time domain analysis is deserved to consider in the future work. It is also the writers' intention that after a liner buffeting analysis of long span bridges under skew winds in the time domain is satisfactorily completed, a nonlinear buffeting analysis in the time domain for the case of skew winds will be explored.

Acknowledgements

The writers are grateful for the financial supports from The Hong Kong Polytechnic University through its Area Strategic Development (ASD) Programme in Wind Effects on Structures, the Research Grants Council of Hong Kong through a RGC research grant (PolyU5155/03E), and the National Natural Science Foundation through a NNSF grant (No.50378068). Sincere thanks should go to the Tsing Ma Control Area Division of Hong Kong Highways Department for providing the writers with the design drawings. The writers would also want to thank Dr J. Chen and Dr. Y.F. Duan of The Hong Kong Polytechnic University for their help in the field measurement data analysis. Any points and concluding remarks presented in this paper are entirely those of the writers.

Appendix A - Expressions of coefficients a_{jk} of oblique bridge deck strip in Eq. (7)

The expressions of coefficients $a_{jk}(j=1,2,...,6;\ k=1,2,...,3)$ in Eq. (7) are given in the following with the subscript "i" omitted (Zhu 2002a)

$$a_{11} = 2C_{C_{\tilde{q}}},\ a_{21} = 2C_{D_{\tilde{p}}},\ a_{31} = 2C_{L_{\tilde{h}}},\ a_{41} = 2BC_{M_{\tilde{\alpha}}},\ a_{51} = 2BC_{M_{\tilde{\gamma}}},\ a_{61} = 2BC_{M_{\tilde{\phi}}} \quad \text{(A-1 a-f)}$$

$$\left.\begin{aligned}
a_{12} &= -s_1 C_{D_{\tilde{p}}} + s_7 C_{L_{\tilde{h}}} + s_2 C'^{\beta}_{C_{\tilde{q}}} + s_3 C'^{\theta}_{C_{\tilde{q}}} \\
a_{22} &= -s_3 C_{L_{\tilde{h}}} + s_1 C_{C_{\tilde{q}}} + s_2 C'^{\beta}_{D_{\tilde{p}}} + s_3 C'^{\theta}_{D_{\tilde{p}}} \\
a_{32} &= -s_7 C_{C_{\tilde{q}}} + s_3 C_{D_{\tilde{p}}} + s_2 C'^{\beta}_{L_{\tilde{h}}} + s_3 C'^{\theta}_{L_{\tilde{h}}} \\
a_{42} &= B(-s_1 C_{M_{\tilde{\gamma}}} + s_7 C_{M_{\tilde{\phi}}} + s_2 C'^{\beta}_{M_{\tilde{\alpha}}} + s_3 C'^{\theta}_{M_{\tilde{\alpha}}}) \\
a_{52} &= B(-s_3 C_{M_{\tilde{\phi}}} + s_1 C_{M_{\tilde{\alpha}}} + s_2 C'^{\beta}_{M_{\tilde{\gamma}}} + s_3 C'^{\theta}_{M_{\tilde{\gamma}}}) \\
a_{62} &= B(-s_7 C_{M_{\tilde{\alpha}}} + s_3 C_{M_{\tilde{\gamma}}} + s_2 C'^{\beta}_{M_{\tilde{\phi}}} + s_3 C'^{\theta}_{M_{\tilde{\phi}}})
\end{aligned}\right\} \quad \text{(A-2 a-f)}$$

$$\left.\begin{aligned}
a_{13} &= -s_4 C_{D_{\bar{p}}} + s_8 C_{L_{\bar{h}}} + s_5 C'^{\beta}_{C_{\bar{q}}} + s_6 C'^{\theta}_{C_{\bar{q}}} \\
a_{23} &= -s_6 C_{L_{\bar{h}}} + s_4 C_{C_{\bar{q}}} + s_5 C'^{\beta}_{D_{\bar{p}}} + s_6 C'^{\theta}_{D_{\bar{p}}} \\
a_{33} &= -s_8 C_{C_{\bar{q}}} + s_6 C_{D_{\bar{p}}} + s_5 C'^{\beta}_{L_{\bar{h}}} + s_6 C'^{\theta}_{L_{\bar{h}}} \\
a_{43} &= B(-s_4 C_{M_{\bar{\gamma}}} + s_8 C_{M_{\bar{\phi}}} + s_5 C'^{\beta}_{M_{\bar{\alpha}}} + s_6 C'^{\theta}_{M_{\bar{\alpha}}}) \\
a_{53} &= B(-s_6 C_{M_{\bar{\phi}}} + s_4 C_{M_{\bar{\alpha}}} + s_5 C'^{\beta}_{M_{\bar{\gamma}}} + s_6 C'^{\theta}_{M_{\bar{\gamma}}}) \\
a_{63} &= B(-s_8 C_{M_{\bar{\alpha}}} + s_6 C_{M_{\bar{\gamma}}} + s_5 C'^{\beta}_{M_{\bar{\phi}}} + s_6 C'^{\theta}_{M_{\bar{\phi}}})
\end{aligned}\right\} \quad \text{(A-3 a-f)}$$

where B is the characteristic width of the bridge deck; $C_{C_{\bar{q}}}$, $C_{D_{\bar{p}}}$, $C_{L_{\bar{h}}}$, $C_{M_{\bar{\alpha}}}$, $C_{M_{\bar{\gamma}}}$ and $M_{M_{\bar{\phi}}}$ are the aerodynamic coefficients of buffeting crosswind force, drag, lift, pitching moment, rolling moment and yawing moment of the bridge deck oblique strip with respect to the local wind coordinate $\overline{qph}$ system, respectively; $(\ )'^{\beta} = \partial(\ )/\partial\bar{\beta}$ and $(\ )'^{\theta} = \partial(\ )/\partial\bar{\theta}$; and $\bar{\beta}$ and $\bar{\theta}$ are mean wind yaw angle in the horizontal plane and the inclination angle in the vertical plane respect to the local wind coordinate $\overline{qph}$ system, respectively.

The coefficients $s_i (i = 1, ..., 8)$ are given as follows

$$\left.\begin{aligned}
s_1 &= (t_{11}t_{22} - t_{21}t_{12})/\sqrt{t_{11}^2 + t_{21}^2} \\
s_2 &= (t_{11}t_{22} - t_{21}t_{12})/(t_{11}^2 + t_{21}^2) \\
s_3 &= t_{32}/\sqrt{t_{11}^2 + t_{21}^2} \\
s_4 &= (t_{11}t_{23} - t_{21}t_{13})/\sqrt{t_{11}^2 + t_{21}^2} \\
s_5 &= (t_{11}t_{23} - t_{21}t_{13})/(t_{11}^2 + t_{21}^2) \\
s_6 &= t_{33}/\sqrt{t_{11}^2 + t_{21}^2} \\
s_7 &= t_{31}(t_{11}t_{22} - t_{21}t_{12})/(t_{11}^2 + t_{21}^2) \\
s_8 &= t_{31}(t_{11}t_{23} - t_{21}t_{13})/(t_{11}^2 + t_{21}^2)
\end{aligned}\right\} \quad \text{(A-4 a-h)}$$

where t_{ij} $(i = 1,2,3; j = 1,2,3)$ is the element of the ith row and jth column of the matrix $\boldsymbol{T}_{LrGw}$.

References

Bathe, K.J. (1982), *Finite Element Procedures in Engineering Analysis*, Prentice-Hall, Englewood Cliffs, N.J.

Bucher, C.G. and Lin, Y.K. (1988), "Stochastic stability of bridges considering coupled modes", *J. Eng. Mech., ASCE*, **114**(12), 2055-2071.

Chen, X.Z., Matsumoto, M. and Kareem, A. (2000a), "Aerodynamic coupling effects on flutter and buffeting of bridges", *J. Eng. Mech., ASCE*, **126**(1), 17-26.

Chen, X.Z., Matsumoto, M. and Kareem, A. (2000b), "Time domain flutter and buffeting response analysis of bridges", *J. Eng. Mech., ASCE*, **126**(1), 7-16.

Davenport, A.G. (1962), "Buffeting of a suspension bridge by storm winds", *J. Struct. Div., ASCE*, **88**(ST3), 233-268.

Deodatis, G. (1996), "Simulation of ergodic multivariate stochastic process", *J. Eng. Mech., ASCE*, **122**(8), 778-787.

Holmes, J.D. (2001), *Wind Loading of Structures*, Spon Press, London.
Jain, A., Jones, N.P. and Scanlan, R.H. (1996), "Coupled flutter and buffeting analysis of long-span bridges", *J. Struct. Eng., ASCE,* **122**(7), 716-725.
Kimura, K. and Tanaka, H. (1992), "Bridge buffeting due to wind with yaw angles", *J. Wind Eng. Ind. Aerodyn*., **41-44**, 1309-1320.
Lau, C.K., Wong, K.Y. and Chan, K.W.Y. (1998), "Preliminary monitoring results of Tsing Ma Bridge", *The 14th Nat. Conf. on Bridge Eng*., Shanghai, **2**, 730-740.
Scanlan, R.H. (1978), "The action of flexible bridges under wind. Part 2: Buffeting theory", *J. Sound Vib*., **60**(2), 201-211.
Scanlan, R.H. and Jones, N.P. (1990), "Aeroelastic analysis of cable-stayed bridges", *J. Struct. Eng., ASCE*, **116**(2), 279-297.
Shinozuka, M. and Deodatis, G. (1991), "Simulation of stochastic processes by spectral representation", *Appl. Mech. Rev*., **44**(4), 191-203.
Xiang, H.F., Liu, C.H. and Gu, M. (1995), "Time-domain analysis for coupled buffeting response of long span bridge", *Proc. of the 9th ICWE*, Wiley Eastern Limited, New Delhi, 881-892.
Xu, Y.L., Ko, J.M. and Zhang W.S. (1997), "Vibration studies of Tsing Ma suspension bridge", *J. Bridge Eng., ASCE*, **2**(4), 149-156.
Xu, Y.L., Sun, D.K., Ko, J.M. and Lin, J.H. (1998), "Buffeting analysis of long span bridges: a new algorithm", *Comput. Struct.*, **68**, 303-313.
Xu, Y.L., Zhu, L.D., Wang, K.Y. and Chan, K.W.Y. (2000), "Field measurement results of Tsing Ma suspension bridge during Typhoon Victor", *J. Struct. Eng. Mech*., **10**(6), 454-559.
Xu, Y.L., Zhu, L.D. and Xiang, H.F. (2003), "Buffeting response of long suspension bridges to skew winds", *Wind & Struct., An Int. J*., **6**(3), 179-196.
Zhu, L.D. (2002a), "Buffeting response of long span cable-supported bridges under skew winds: field measurement and analysis", *PhD Dissertation*, the Hong Kong Polytechnic University, Hong Kong.
Zhu, L.D., Xu, Y.L., Zhang, F. and Xiang, H.F. (2002b), "Tsing Ma bridge deck under skew winds-Part I: Aerodynamic coefficients", *J. Wind Eng. Ind. Aerodyn*., **90**, 781-805.
Zhu, L.D., Xu, Y.L. and Xiang, H.F. (2002c), "Tsing Ma bridge deck under skew winds - Part II: flutter derivatives", *J. Wind Eng. Ind. Aerodyn.*, **90**, 807-837.

CC